Available online at www.sciencedirect.com

ScienceDirect

Geochimica et Cosmochimica Acta 198 (2017) 338–359

Geochimica et Cosmochimica Acta

www.elsevier.com/locate/gca

Solute transport into the Jiulong River estuary via pore water exchange and submarine groundwater discharge: New insights from $^{224}Ra/^{228}Th$ disequilibrium

Qingquan Hong, Pinghe Cai *, Xiangming Shi, Qing Li, Guizhi Wang

State Key Laboratory of Marine Environmental Science, Xiamen University, Xiamen 361005, PR China
College of Ocean and Earth Sciences, Xiamen University, Xiamen 361005, PR China

Received 17 April 2016; accepted in revised form 5 November 2016; Available online 16 November 2016

Abstract

Pore water exchange (PEX) and submarine groundwater discharge (SGD) represent two mechanisms for solute transport from the seabed into the coastal ocean. However, their relative importance remains to be assessed. In this study, we pursued the recently developed $^{224}Ra/^{228}Th$ disequilibrium approach to quantify PEX fluxes of ^{224}Ra into the Jiulong River estuary, China. By constructing a full mass balance of water column ^{224}Ra, we were allowed to put various source terms, i.e., SGD, diffusive and advective pore water flow (PEX), and river input in a single context. This led to the first quantitative assessment of the relative importance of PEX vs. SGD in the delivery of solutes into an estuary. We carried out two surveys in the Jiulong River estuary: one in January 2014 (winter survey), the other in August 2014 (summer survey). By virtue of a 1-D mass balance model of ^{224}Ra in the sediment column, we demonstrated that PEX fluxes of ^{224}Ra were highly variable, both temporally and spatially, and can change by 1–2 orders of magnitude in our study area. Moreover, we identified a strong correlation between ^{224}Ra-based irrigation rate and ^{234}Th-based sediment mixing rate. Our results highlighted irrigation as the predominant PEX process for solute transfer across the sediment–water interface.

Total PEX flux of ^{224}Ra (in 10^{10} dpm d^{-1}) into the Jiulong River estuary was estimated to be 22.3 ± 3.0 and 33.7 ± 5.5 during the winter and summer surveys, respectively. In comparison, total SGD flux of ^{224}Ra (in 10^{10} dpm d^{-1}) was 11.3 ± 8.6 and 49.5 ± 16.3 in the respective seasons. By multiplying the PEX fluxes of ^{224}Ra by the ratio of the concentration gradients of component/^{224}Ra at the sediment–water interface, we quantified the total PEX fluxes of dissolved inorganic carbon (DIC) and nutrients (NH_4^+, NO_3^-, and H_4SiO_4) into the Jiulong River estuary. In the meantime, net export of DIC and nutrients via SGD were estimated by multiplying the SGD fluxes of ^{224}Ra by the DIC (nutrients)/^{224}Ra ratios in the SGD end-members around this area. Our results revealed that PEX-driven fluxes of solutes rival net SGD input and river input in an estuary. An additional new finding is that water column NO_3^- in the surface estuary was effectively sequestered due to SGD, probably as a result of intense denitrification occurring in the anoxic subterranean estuary.

Keywords: Pore water exchange; Submarine groundwater discharge; Irrigation; $^{224}Ra/^{228}Th$ disequilibrium; Jiulong River estuary

1. INTRODUCTION

Submarine groundwater discharge (SGD) is referred to as "the flow of water through continental margins from the seabed to the coastal ocean, with scale lengths of meters to kilometers, regardless of fluid composition and driving force" (Burnett et al., 2003; Moore, 2010). Since Moore

* Corresponding author at: State Key Laboratory of Marine Environmental Science, Xiamen University, Xiamen 361005, PR China. Fax: +86 592 2180655.
E-mail address: Caiph@xmu.edu.cn (P. Cai).

http://dx.doi.org/10.1016/j.gca.2016.11.002
0016-7037/

and coworkers provided the first evidence of large SGD fluxes into the coastal ocean in the mid-1990s (Moore, 1996; Rama and Moore, 1996), SGD studies have drawn continuous interest from numerous researchers, leading to the rapid emergence of this field in the past two decades. Now it is generally believed that SGD is not only an important component of the hydrological cycle, but also a major source of carbon, nutrients, trace metals, and natural radionuclides to the coastal ocean (e.g., Moore and Shaw, 1998; Shaw et al., 1998; Charette et al., 2001; Cai et al., 2003; Moore et al., 2008; Santos et al., 2009; Dulaiova et al., 2010; Beck et al., 2013; Beusen et al., 2013; Garcia-Orellana et al., 2013; Rodellas et al., 2015a).

The magnitude of SGD fluxes into the coastal ocean is generally assessed using the naturally occurring radium isotopes: ^{228}Ra ($t_{1/2} = 5.75$ yr), ^{226}Ra ($t_{1/2} = 1600$ yr), ^{224}Ra ($t_{1/2} = 3.66$ d), and ^{223}Ra ($t_{1/2} = 11.4$ d), which are commonly quoted as the radium quartet (e.g., Rama and Moore, 1996). A major advantage of the radium quartet as a tracer of SGD is that radium is highly enriched in saline coastal groundwater, such that small inputs of SGD can be recognized as a strong signal. In addition, the wide range of their half-lives allows to trace processes occurring over a variety of time scales and to quantify multiple sources of SGD. In practice, the radium approach generally involves the construction of a Ra mass balance in the study area. To successfully quantify the SGD flux with the radium approach, it is essential to accurately constrain all the supply and loss terms of Ra other than SGD. Supply terms in the Ra mass balance include riverine discharge, desorption of Ra from suspended particles, regeneration and release from bottom sediments, as well as inputs associated with SGD. Loss terms of Ra include radioactive decay and export to the open ocean.

Bottom sediments represent a continuous source of Ra isotopes to the water column. This source may be particularly important for the short-lived ^{224}Ra and ^{223}Ra because of their rapid regeneration rates in the near-surface sediments (e.g., Garcia-Orellana et al., 2014; Rodellas et al., 2015b). Transfer of radium isotopes across the sediment–water interface could take place through a variety of processes with scale lengths of "milli-meters to meters", like molecular diffusion, flow- and topography-induced advection, wave pumping, ripple migration, shear flow, as well as shallow bio-turbation and bio-irrigation (e.g., Santos et al., 2012). These small scale processes are collectively referred to as "pore water exchange" (PEX), as opposed to the definition of SGD with scale lengths of "meters to kilometers" (e.g., Santos et al., 2012; Garcia-Orellana et al., 2014; Rodellas et al., 2015b). However, quantifying fluxes of Ra isotopes induced by PEX is difficult, due primarily to limitations inherent to the traditional approaches, i.e., the incubation method and the modeling approach. The incubation method is problematic because it is rather unrealistic to simulate the complex in-situ conditions near the sediment–water interface, particularly in the dynamic coastal seas. The modeling approach generally invokes a line of assumptions, which are not always valid or even unjustified (e.g., Berner, 1980).

Recently, we have developed a novel method, termed "the ^{224}Ra/^{228}Th disequilibrium approach", to quantify benthic fluxes of DO (dissolved oxygen), DIC, and NH_4^+ in a coastal sea (Cai et al., 2014, 2015). This method is unique in that it does not impose any interference on the system. As such, it is regarded as the most reliable means of quantifying benthic fluxes of ^{224}Ra and other regenerated components into the coastal ocean. Another advantage is that compared to the traditional incubation method, the ^{224}Ra/^{228}Th disequilibrium approach allows a much higher sampling resolution in the highly heterogeneous coastal sediments. In the present study, we pursue this method to assess the relative importance of PEX vs. SGD, the latter of which is commonly viewed as a pathway of "new" materials, in the delivery of DIC and nutrients into an estuary. In so doing, the ^{224}Ra/^{228}Th disequilibrium approach is utilized to quantify PEX fluxes of ^{224}Ra and other regenerated components into the Jiulong River estuary, China. Subsequently, by constructing a full mass balance of water column ^{224}Ra, the derived ^{224}Ra fluxes are used to constrain the SGD input in the system. Our study provides a general approach for quantifying the relative contribution of inputs of autochthonous vs. allochthonous components into a coastal system.

2. SAMPLING AND ANALYTICAL METHODS

2.1. Study area

The Jiulong River is located in the southeast China and flows through the Jiulong River estuary into the southern Taiwan Strait (Fig. 1). Annual discharge rates of water and sediment from the Jiulong River are 1.4×10^{10} m^3 yr^{-1} and 2.2×10^6 t yr^{-1} respectively, most of which (~75%) takes place in the wet season, from April to October. The estuary traps most of the discharged riverine particles, leading to the formation of a submerged delta (Xu and Li, 2003). Bottom sediments along the southern boundary and in the lower estuary are silt and clay. In comparison, sediments in the mid-estuary are characterized by a mixture of sand and silt. Overall, fine-grained sediments occupy ~60% of the total area of the estuary (Wang, 2008). This region is strongly affected by semidiurnal tides and the tidal current speed can be >2 m s^{-1}. Over an annual scale, the average residence time of water mass in the estuary was estimated to be 2 days based on water and salt budgets (Cao et al., 2005).

Polychaetes, mollusks and crustacea are the main benthic fauna in the Jiulong River estuary. The benthic community is dominated by polychaetes in spring and summer. In contrast, it is dominated by mollusks in fall and winter. The biomass of the benthic fauna averages 56 g m^{-2} and shows little seasonal variation (He et al., 1988).

2.2. Sample collection

Samples were collected along the salinity gradient within the Jiulong River estuary (Fig. 1) in January (winter) and August (summer), 2014. Detailed information about the sampling stations is presented in Appendix T1. Undisturbed sediment cores were collected using a standard box corer ($30 \times 30 \times 60$ cm^3). Immediately after sample retrie-

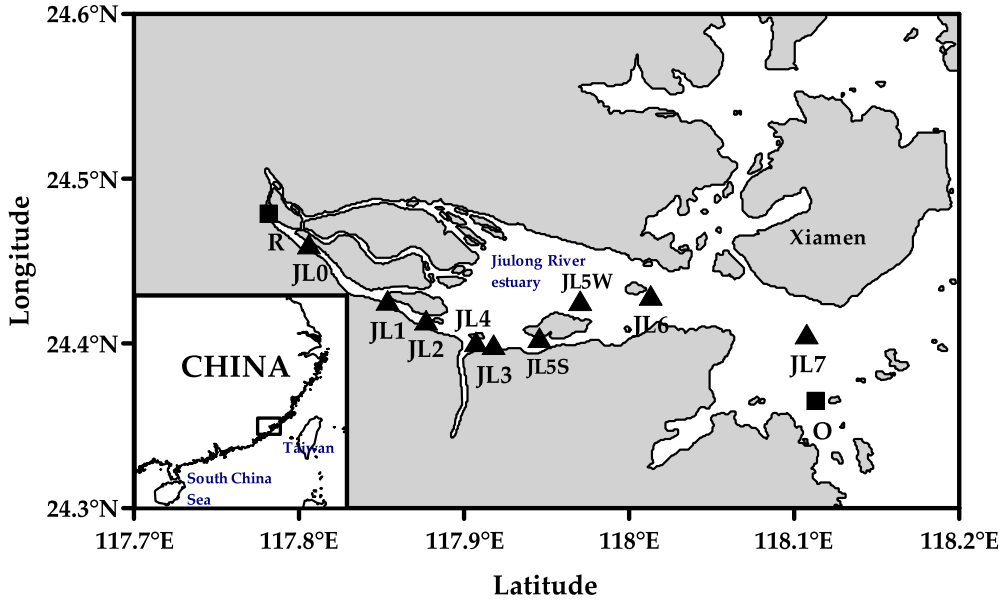

Fig. 1. Sampling locations in the Jiulong River estuary. Solid square: stations where only water samples were collected; Solid triangle: stations where both sediment and water samples were collected. Note that St. JL5 was occupied at different location in the winter and summer surveys, and was distinguished by postfixes W and S.

val, temperature and salinity of the overlying seawater were measured. An aliquot of ~4 l of overlying seawater in the box corer was filtered through a 142-mm GFF filter to derive the ^{224}Ra and ^{228}Th activities in suspended particles. Sediment sub-cores were taken by inserting PVC tubes with a diameter of 47 mm or 65 mm into the bulk sediment. Pore water for ^{224}Ra, DIC, and nutrient analyses was extracted from sediment sub-cores using a Rhizon sampler (Seeberg-Elverfeldt et al., 2005).

Surface and bottom water samples were collected for the analyses of ^{224}Ra, DIC, and nutrients using a Niskin bottle. In the summer survey, TSM (total suspended matter) samples were also collected. Seawater ^{224}Ra was pre-concentrated and measured on a delayed coincidence counter (the RaDeCC system) according to the method described in Moore and Arnold (1996). DIC samples were preserved with saturated $HgCl_2$ solution onboard. Nutrient samples were filtered onboard through a 0.45 μm pore size cellulose acetate membrane and poisoned with 1–2‰ chloroform. Duplicated samples for NO_3^- and NO_2^- (hereafter referred to as NO_3^-) analyses were frozen at −20 °C while NH_4^+ and dissolved silicate (H_4SiO_4) samples were stored at 4 °C.

2.3. Analyses of ^{224}Ra and ^{228}Th

Analyses of ^{224}Ra and ^{228}Th in sediment and suspended particles are based on the method described in Cai et al. (2012). Briefly, a sediment sub-core was sliced into 1 cm thick slabs. Milli-Q water was added and the sample was sonicated to generate a slurry in an ultrasonic bath. After adjusting the pH of the slurry to 8.0–9.0, $KMnO_4$ and $MnCl_2$ solutions were added. With the formation of a MnO_2 suspension, ^{224}Ra in dissolved phase was co-precipitated. The slurry together with MnO_2 suspension was filtered evenly onto a 142 mm GFF filter. Subsequently, the sample was counted on a RaDeCC system for 4–6 h. After 8–10 days and ~25 days, the sample was re-measured in the same RaDeCC system. ^{224}Ra and ^{228}Th activities in bulk sediment (hereafter referred to as total ^{224}Ra and ^{228}Th) can be calculated either from the first and second measurements, or from the first and third measurements.

For the analysis of pore water ^{224}Ra, an aliquot of ~20–30 ml of pore water was extracted from sediment sub-cores at discrete depths. A certain volume of Milli-Q water was added to the sample. After adjustment of the pH, $KMnO_4$ and $MnCl_2$ solutions were added to form a suspension of MnO_2 to co-precipitate ^{224}Ra. The MnO_2 precipitate was filtered onto a 142 mm GFF filter and counted on a RaDeCC system for 10 h. Detection efficiency of the counter was calibrated with a ^{232}U-^{228}Th standard prepared in the same manner as the pore water sample.

2.4. Analyses of excess ^{234}Th ($^{234}Th_{ex}$)

Sediment cores for $^{234}Th_{ex}$ measurements were collected only during the winter survey. $^{234}Th_{ex}$ activity in bulk sediment was acquired in a manner similar to that described in Cai et al. (2014). A sediment sub-core was sliced in an interval of 0.5–2 cm from the surface to a depth of 10 cm. The sediment samples were dried and leached with a mixture of 6 N HCl + H_2O_2 solution for 3 times. The leachate was then purified on an anion-exchange column. ^{234}Th was co-precipitated with MnO_2 suspension and counted on a gas-flow proportional low-level beta counter (GM-25–5, RISØ National Laboratory, Denmark). After 5–6 months, a parallel sediment sample was processed in the same manner as the initial sample to obtain the ^{238}U-supported ^{234}Th activity, which

was subtracted from the first measurement to calculate the $^{234}Th_{ex}$ activity (dpm g^{-1}).

2.5. Analyses of DIC, nutrients and TSM

Within 24 h after sample collection, DIC was determined by acidification of ~0.5 ml aliquot and subsequent quantification of CO_2 with an infrared analyzer (Appolo Dissolved Inorganic Carbon Analyzer). This method has a precision of 0.1–0.2% (Cai et al., 2004). NO_3^- was determined with an AA3 Auto-Analyzer (Bran-Lube GmbH) following the classical colorimetric methods (Dai et al., 2008). NH_4^+ and H_4SiO_4 were analyzed on a flow injection analyzer (Tri-223 Auto-Analyzer) using the indophenol blue spectrophotometric method and the silicon molybdenum blue method (Pai et al., 2001). The detection limits were 0.1, 0.04, 0.5 and 0.08 μmol l^{-1} for NO_3^-, NO_2^-, NH_4^+ and H_4SiO_4, respectively.

TSM was determined by filtering ~500 ml of seawater onto a pre-weighed Nuclepore filter (0.45 μm pore size). The filter was rinsed by Milli-Q water and dried to a constant weight at 60 °C. The content of TSM was calculated from the weight difference between the sample and the filter.

2.6. Sediment porosity

Wet sediment samples were dried at 60 °C to a constant weight. Porosities were calculated from the weight loss using a grain density of 2.6 g cm^{-3} and corrected for the salt content.

3. RESULTS

Sediment porosity (ϕ), DIC, nutrients (NO_3^-, NH_4^+, H_4SiO_4) and ^{224}Ra ($^{224}Ra_P$) in pore water, as well as total ^{224}Ra ($^{224}Ra_T$), ^{228}Th and $^{234}Th_{ex}$ activities in the near-surface sediments of the Jiulong River estuary are listed in Appendix T1. Also listed are temperature (T), salinity (S), and TSM concentrations of the bottom water. ^{224}Ra and ^{228}Th activities are reported with an error that was propagated from counting statistics, detector calibration, chance coincidence correction, and decay/ingrowth correction. The uncertainty associated with $^{234}Th_{ex}$ activities includes the two parallel measurements in the beta counter, the error of detector calibration, as well as the standard error of the overall yields. We compared the first and second measurements (^{228}Th-2nd) and the first and third measurements (^{228}Th-3rd), and found excellent agreement between the ^{228}Th-2nd and ^{228}Th-3rd activities (mean ratio of ^{228}Th-3rd/^{228}Th-2nd = 0.992 ± 0.059, 1SD, n = 185). This strongly suggests that our protocol for determination of ^{224}Ra and ^{228}Th in sediments is very reliable, and that our RaDeCC systems are also quite stable. As such, we believe that the difference between ^{224}Ra and ^{228}Th activities as shown in Appendix T1 is a real reflection of the deviation of ^{224}Ra relative to ^{228}Th in estuarine sediments. It should be noted that the final ^{228}Th activities presented in Appendix T1 are the averages of ^{228}Th-2nd and ^{228}Th-3rd.

3.1. Distributions of ^{228}Th and ^{224}Ra

3.1.1. Depth distributions of ^{228}Th and ^{224}Ra in sediments

Vertical distributions of pore water ^{224}Ra, $^{224}Ra_T$, ^{228}Th, as well as $^{224}Ra_T/^{228}Th$ ratio in the upper 0–25 cm sediment in the Jiulong River estuary are illustrated in Fig. 2. During the winter and summer surveys, activity of ^{228}Th in sediment fell in the range of 1.24 ± 0.03–6.18 ± 0.16 dpm g^{-1} and 1.36 ± 0.03–7.13 ± 0.18 dpm g^{-1}, respectively. There was a general trend of decreasing ^{228}Th activity in the surface sediment with distance downstream off the river mouth. Overall, ^{228}Th activity was relatively low in the topmost 0–1 cm sediment. During the summer survey, ^{228}Th activity at St. JL1 and JL7 decreased from the surface to a relatively constant value at depth. This could be due to the combined effect of ^{228}Th supply via sinking particles from the overlying water column and a loss of its dissolvable progenitor, ^{228}Ra, from the upper sediment column (Bernat and Goldberg, 1968).

As ^{224}Ra is produced by the decay of ^{228}Th, $^{224}Ra_T$ showed a distribution pattern similar to ^{228}Th (Fig. 2). During the winter and summer surveys, $^{224}Ra_T$ activity varied from 1.21 ± 0.04 to 6.01 ± 0.16 dpm g^{-1}, and from 1.40 ± 0.04 to 6.04 ± 0.17 dpm g^{-1}, respectively. In the winter survey, a marked deficit of ^{224}Ra relative to ^{228}Th was evident down to a depth of 20 cm in the upper estuary, indicating intense migration of ^{224}Ra out of the sediment. In the lower estuary, $^{224}Ra_T/^{228}Th$ ratio exhibited relatively large spatial and seasonal variations. At St. JL3, a deficit of ^{224}Ra was notable only in the topmost 0–1 cm sediment in both seasons. During the winter survey, ^{224}Ra was found to be in secular equilibrium with ^{228}Th throughout the sediment column at St. JL5 and JL6. In comparison, a significant deficit of ^{224}Ra relative to ^{228}Th was evident down to a depth of 20 cm sediment at St. JL6 in the summer. During the summer survey, an extra station (JL4) was occupied. A significant deficit of ^{224}Ra was observed in the upper 6 cm sediment at this station.

Activity of ^{224}Ra in pore water fell in the range of 6.3 ± 3.0–119 ± 8.1 dpm l^{-1} during the winter survey, and of 1.1 ± 2.0–108 ± 5.5 dpm l^{-1} during the summer survey. These values are ~1–2 orders of magnitude higher than those in the bottom water. Nevertheless, they account for <5% of the total ^{224}Ra in the sediment. Low activities of ^{224}Ra in pore water were generally observed near the river mouth where salinity was low and ^{224}Ra tends to be bounded onto sediment particles (Fig. 2). As salinity increased, some ^{224}Ra desorbed (Swarzenski et al., 2003), leading to an increase in pore water ^{224}Ra activity with distance downstream off the river mouth.

3.1.2. Distributions of ^{228}Th and ^{224}Ra in the water column

During the winter and summer surveys, seawater ^{224}Ra activity varied from 35 ± 1.5 to 228 ± 6.5 dpm 100 l^{-1} and from 19 ± 1.0 to 181 ± 3.9 dpm 100 l^{-1}, respectively (see Appendix T1 and Appendix T2). Seawater ^{224}Ra activity peaked in the mid-salinity region (Fig. 3), resembling the pattern reported in prior studies (e.g., Wang et al., 2015). In the respective seasons, activity of ^{228}Th in suspended particles decreased from 4.7 ± 0.12 and 6.4 ± 0.18 dpm g^{-1} at

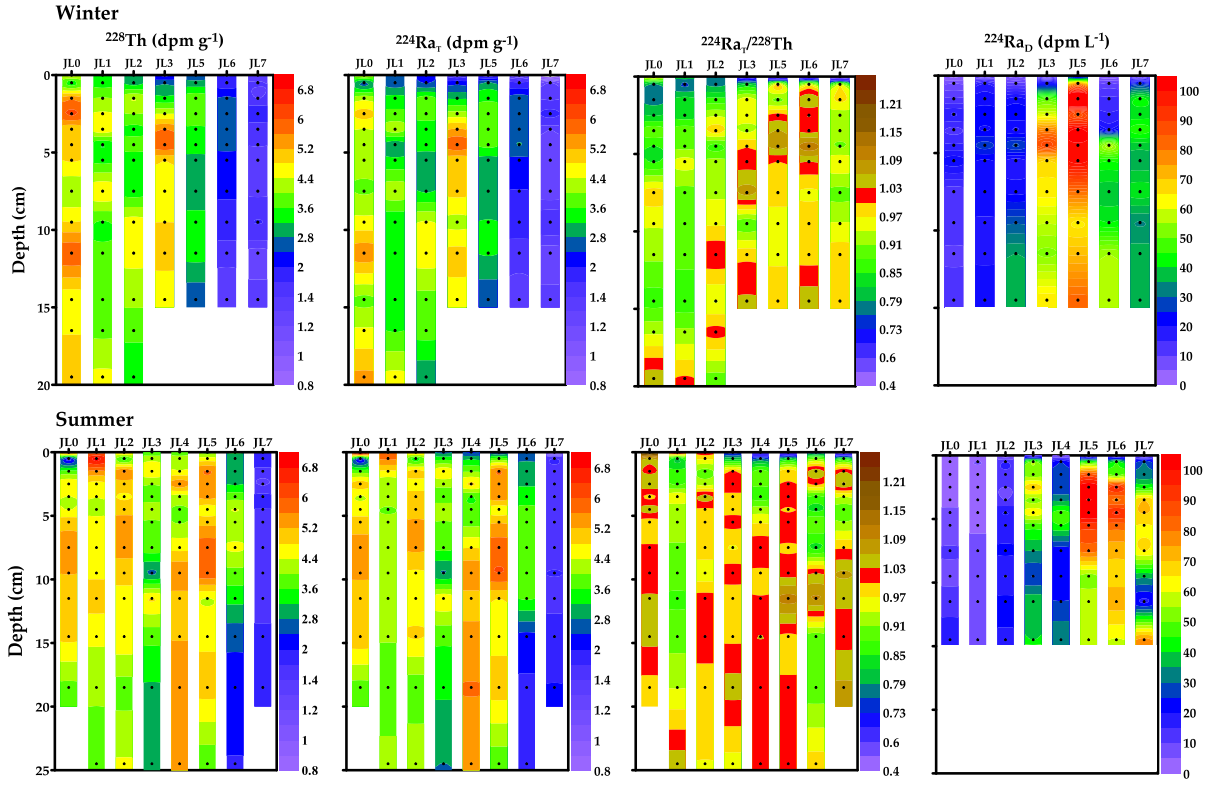

Fig. 2. Vertical distribution of ^{228}Th, ^{224}Ra$_T$, ^{224}Ra$_T$/^{228}Th ratio in bulk sediment and dissolved ^{224}Ra in pore water (upper panels: winter survey; lower panels: summer survey). Ratios of ^{224}Ra$_T$/^{228}Th <1.00 denote a deficit of ^{224}Ra relative to ^{228}Th.

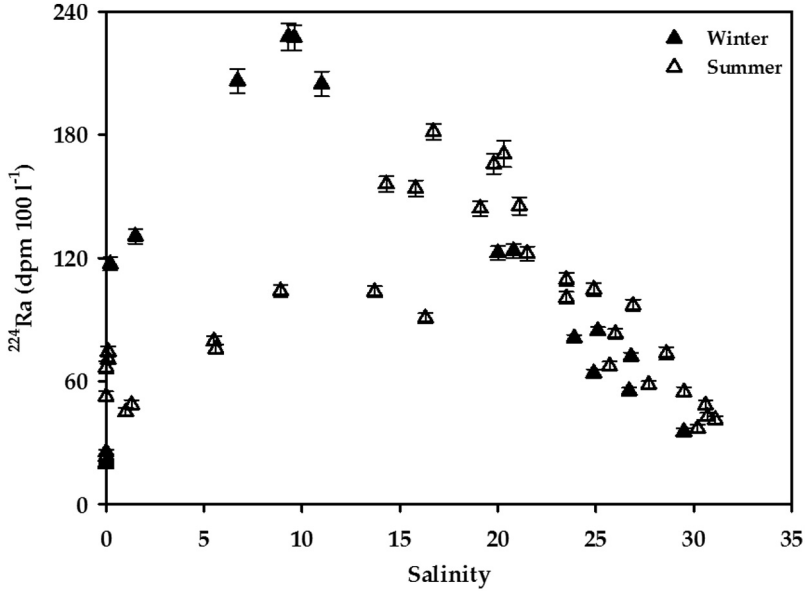

Fig. 3. ^{224}Ra activities in seawater along the salinity gradient in the Jiulong River estuary.

the innermost station to 1.4 ± 0.04 and 1.8 ± 0.06 dpm g^{-1} at the outermost station (Fig. 4). Activity of ^{224}Ra in suspended particles followed a similar pattern, dropping from 4.7 ± 0.12 and 8.0 ± 0.21 dpm g^{-1} at St. JL0 to 0.58 ± 0.03 and 0.90 ± 0.04 dpm g^{-1} at St. JL7. In the low salinity region ($S < 2$), ^{224}Ra on suspended particles was either in slight excess or in secular equilibrium with ^{228}Th. However, as mixing into seawater, ^{224}Ra/^{228}Th ratio in suspended particles dropped to a relatively constant value of ~0.6–0.7 in the salinity range of 2–25. At $S = 29$, it further attenuated to a minimum of 0.42 ± 0.02. Overall, the average ^{224}Ra/^{228}Th ratio in suspended particles at $S > 2$ is 0.61 $\pm$ 0.13 (1SD, $n = 11$), indicating that ~40% of ^{224}Ra in suspended particles desorbed during mixing into seawater.

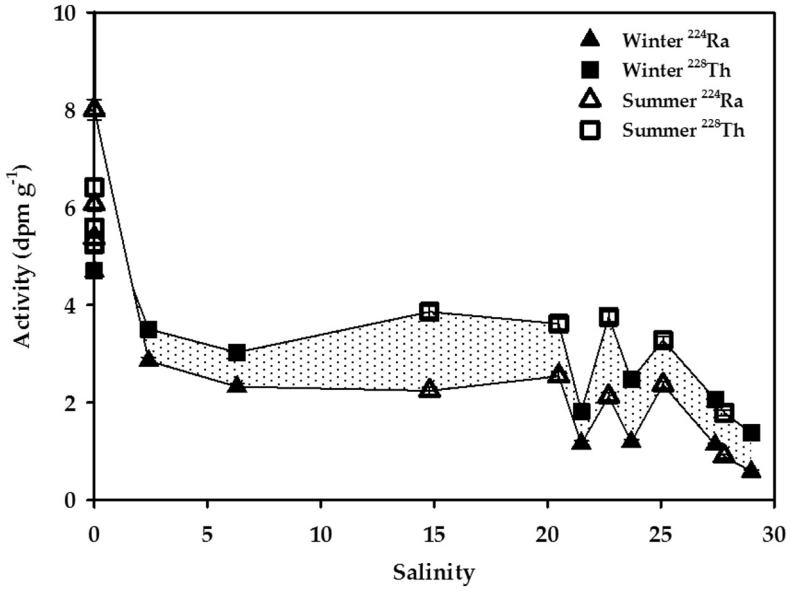

Fig. 4. ^{224}Ra and ^{228}Th activities in suspended particles in the Jiulong River estuary. The shadowed area denotes the deficiency of ^{224}Ra relative to ^{228}Th.

3.2. Depth distribution of $^{234}Th_{ex}$

During the winter survey, $^{234}Th_{ex}$ penetrated into a depth of 2–10 cm sediment (see Appendix T1). Activity of $^{234}Th_{ex}$ fell in the range of 0.00 ± 0.08–2.86 ± 0.20 dpm g^{-1}. As shown in Fig. 5, it generally diminished rapidly with depth due to the combined effect of decay and sediment mixing after deposition on the seabed. An exception is at St. JL0, where $^{234}Th_{ex}$ increased from the sediment surface to a depth of 2–3 cm and below, it approached zero at a depth of ~10 cm.

3.3. Distributions of DIC and nutrients

Vertical distributions of pore water DIC, NO_3^-, NH_4^+ and H_4SiO_4 in the upper 0–15 cm sediment column are illustrated in Fig. 6. Overall, depth profiles of these dissolved constituents in pore water are a typical manifestation of early diagenetic reactions associated with organic matter remineralization. Concerning the early diagenesis, one of the fundamental concepts is that given an initial set of natural oxidants in sediments, biogeochemical redox reactions follow a regular progression with time, in many cases equivalent to depth. Naturally occurring oxidants, i.e., O_2, NO_3^-, MnO_2, Fe_3O_4, SO_4^{2-}, and CO_2, are consumed sequentially as a function of free energy yield. Consequently, concentrations of DIC, NH_4^+ and H_4SiO_4 in pore water typically increase with depth, and there are generally strong correlations among these constituents. In contrast, NO_3^- is depleted in anoxic interstitial waters due to a diagenetic process termed denitrification. Spatial and temporal variability of pore water components, in the meantime, is determined by the relative fluxes of oxidants and reductants, diffusive transport, and advection rates of materials away from the sediment–water interface (e.g., Froelich et al., 1979). Indeed, during the winter survey, DIC and NH_4^+ contents varied from 1090 to 19,340 μmol l^{-1} and from 38 to 1220 μmol l^{-1}, respectively. In comparison, during the summer survey they fell in the range of 2070–30,560 μmol l^{-1} and of 118–4520 μmol l^{-1}, respectively. The average concentrations of DIC and NH_4^+ in the summer (12,000 and 1090 μmol l^{-1}, respectively) were approximately twice those in the winter (6280 and 436 μmol l^{-1}, respectively). High DIC and NH_4^+ contents in pore water were generally observed near the river mouth. In addition, both DIC and NH_4^+ displayed an increasing trend with depth. In contrast to DIC and NH_4^+, NO_3^- and H_4SiO_4 did not display clear seasonality between these two surveys. H_4SiO_4 concentration varied from 112 to 492 μmol l^{-1} and from 48 to 498 μmol l^{-1} during the winter and summer surveys, respectively. Similar to DIC and NH_4^+, H_4SiO_4 concentration was

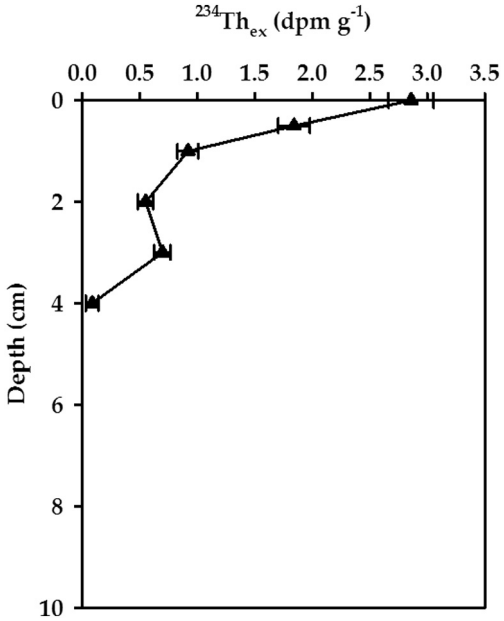

Fig. 5. Typical distribution of $^{234}Th_{ex}$ in the near-surface sediment at St. JL6.

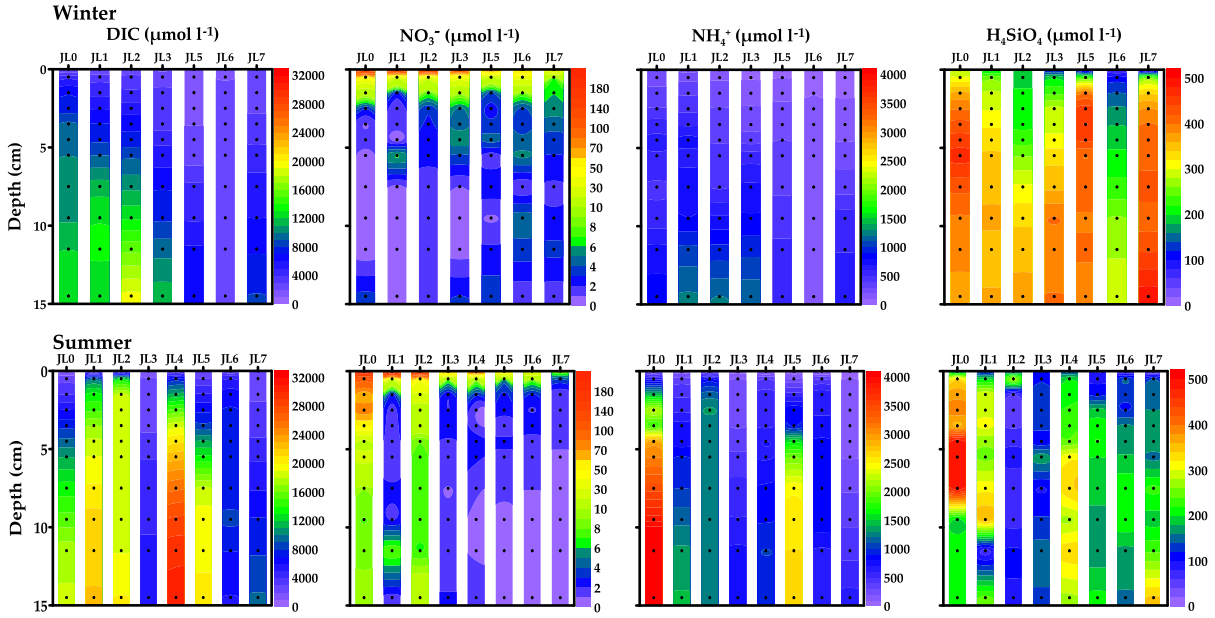

Fig. 6. Vertical distribution of pore water DIC and nutrients in the near-surface sediment of the Jiulong River estuary (upper panels: winter survey; lower panels: summer survey).

generally higher at the river mouth, and showed an increasing trend with depth in the sediment column. For the winter and summer surveys, NO_3^- varied from 0 to 41 μmol l^{-1} and from 0.51 to 105 μmol l^{-1}, respectively. In contrast to DIC, NH_4^+ and H_4SiO_4, NO_3^- was generally depleted below a depth of ~3–7 cm. Two exceptions are St. JL0 and JL2 occupied during the summer survey, where NO_3^- can penetrate into a depth of 15 cm.

Fig. 7 shows the distributions of DIC, NO_3^-, NH_4^+ and H_4SiO_4 vs. salinity in the overlying waters within the Jiulong River estuary. During the winter and summer surveys, DIC concentration increased from 1299 and 703 μmol l^{-1} at the river mouth to 2021 and 1984 μmol l^{-1} at the outermost station, respectively (see Appendix T1 and Appendix T2). It is evident from Fig. 7 that DIC concentrations increased with salinity and fell above the conservative mixing line at $S < 15$, indicating the existence of an extra source of DIC in this region. In contrast to DIC, nutrient concentrations generally declined with salinity. As mixing into seawater, NO_3^- concentration dropped from 162 to 43 μmol l^{-1} during the winter survey, and from 237 to 2.1 μmol l^{-1} during the summer survey. Concentration of NH_4^+ declined from 205 to 3.6 μmol l^{-1}, and from 144 to 1.5 μmol l^{-1} in the respective seasons. H_4SiO_4 concentration decreased from 288 to 35 μmol l^{-1} during the winter survey, and from 291 to 8.6 μmol l^{-1} during the summer survey. Overall, H_4SiO_4 showed a decreasing trend similar to NO_3^- downstream the estuary.

4. DISCUSSION

4.1. Benthic fluxes of ^{224}Ra induced by pore water exchange (PEX)

4.1.1. Estimation of ^{224}Ra fluxes

PEX fluxes of ^{224}Ra in the Jiulong River estuary were estimated using a 1-D mass balance model (Cai et al., 2012). At steady state, an integration of the ^{224}Ra deficit in the sediment column gives:

$$F_{Ra} = \lambda_{Ra} \int_0^z (A_{Th} - A_{Ra}) dz \quad (1)$$

where F_{Ra} (dpm cm^{-2} d^{-1}) represents ^{224}Ra flux induced by pore water exchange ("+": upward), λ_{Ra} is the decay constant of ^{224}Ra (0.189 d^{-1}), z is the depth below which ^{224}Ra and ^{228}Th are constantly in secular equilibrium, A_{Th} and A_{Ra} denote the activities of ^{228}Th and total ^{224}Ra in sediment (unit: dpm cm^{-3}), respectively.

^{224}Ra fluxes varied from -0.047 ± 0.036 to 1.25 ± 0.13 dpm cm^{-2} d^{-1} during the winter survey, and from -0.100 ± 0.088 to 0.891 ± 0.092 dpm cm^{-2} d^{-1} during the summer survey (Table 1). It should be emphasized that the lower bounds of these estimates are, within uncertainty ($\pm 2\sigma$), indiscernible from zero. The upper bounds are comparable to our previous results in the Yangtze River estuary and the Pearl River estuary (e.g., Cai et al., 2014, 2015). However, they are 1–2 orders of magnitude higher than prior estimates based on the traditional incubation method and the modeling approach (e.g., Beck et al., 2007; Garcia-Orellana et al., 2014; Rodellas et al., 2015a). This difference is mostly likely due to the fact that the incubation method and the modeling approach do not incorporate two major mechanisms for controlling solute transfer across the sediment–water interface, i.e., sediment mixing and irrigation (see the next section).

4.1.2. Transport processes regulating PEX fluxes of ^{224}Ra

Transfer of ^{224}Ra across the sediment–water interface is regulated by a variety of processes, which include molecular diffusion, sediment mixing and irrigation (e.g., Cai et al., 2014, 2015). The relative importance of these processes can be evaluated by comparing the theoretical fluxes of ^{224}Ra induced by molecular diffusion and sediment mixing

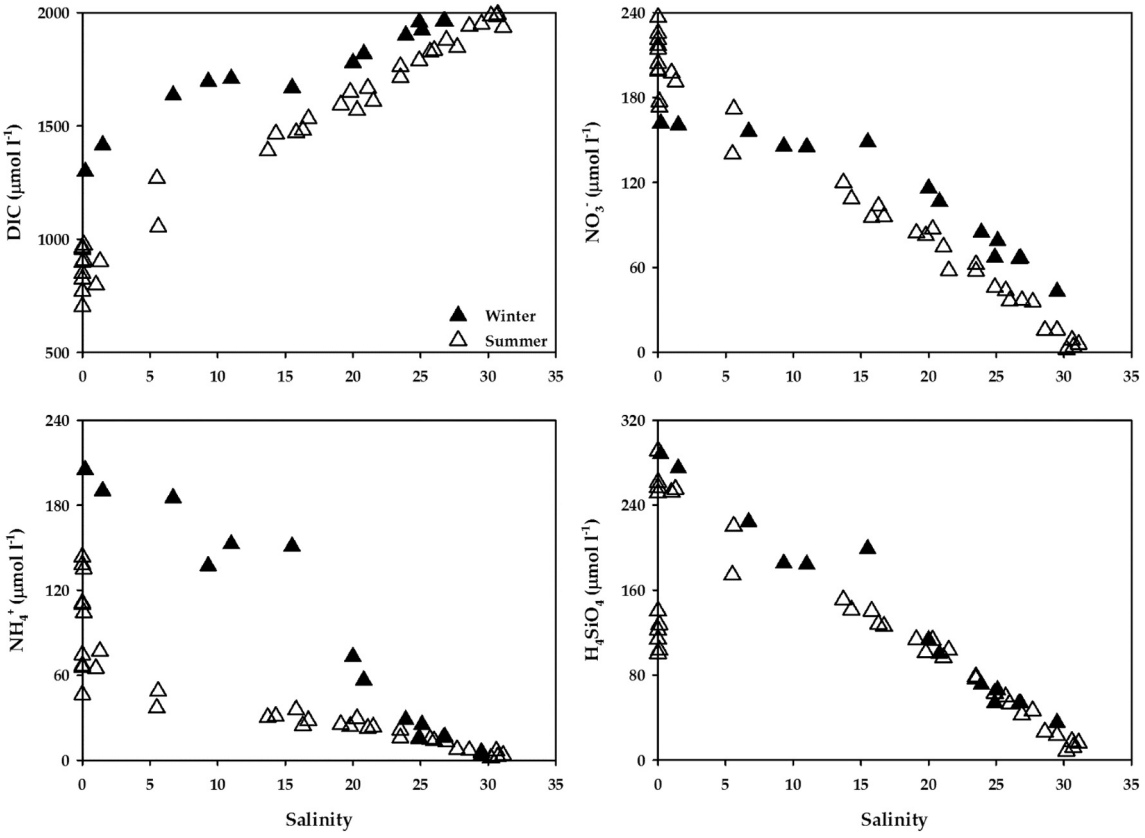

Fig. 7. Distribution of DIC and nutrients vs. salinity in the overlying waters within the Jiulong River estuary.

with the observed deficit of ^{224}Ra relative to ^{228}Th in the sediment column. ^{224}Ra flux induced by molecular diffusion (F_M) can be calculated using Fick's first law (Berner, 1980; Boudreau, 1997):

$$F_M = \phi D_S^{Ra} \frac{\partial^{224}Ra_P}{\partial z} \quad (2)$$

where ϕ represents the porosity of the sediment; D_S^{Ra} is the diffusion coefficient of ^{224}Ra in the sediment, which can be estimated from the diffusivity of ^{224}Ra in seawater (D_{SW}^{Ra}) by correcting for sediment tortuosity (θ) with the relations $D_S^{Ra} = D_{SW}^{Ra}/\theta^2$ and $\theta^2 = 1–2\ln\ \phi$ (Boudreau, 1997; Schulz and Zabel, 2006). The term $\frac{\partial^{224}Ra_P}{\partial z}$ refers to the concentration gradient of dissolved ^{224}Ra at the sediment–water interface. In practice, it is calculated from ^{224}Ra measurements in the bottom water and in pore water of the topmost 0–1 cm sediment. Our results show that during the winter and the summer surveys, F_M varied from 0.003 ± 0.002 to 0.037 ± 0.002 dpm cm^{-2} d^{-1} and from 0.001 ± 0.001 to 0.043 ± 0.004 dpm cm^{-2} d^{-1}, respectively (Table 1). On average, it accounted for <10% of the observed deficit of ^{224}Ra. This value is close to the previous estimates in the Yangtze River estuary and the Pearl River estuary (Cai et al., 2014, 2015), and confirms the notion that molecular diffusion usually plays a minor role in regulating the benthic fluxes of ^{224}Ra in an estuary. Nonetheless, for some locations where the benthic fluxes of ^{224}Ra derived from the deficit of ^{224}Ra in the sediment column were low and thus associated with a large uncertainty, molecular diffusion could be a predominant mechanism for solute transfer across the sediment–water interface. This might be the case for St. JL5 and JL6 occupied during the winter survey, and for St. JL0 and JL5 covered during the summer survey (Table 1).

Dissolved and surface-bound species in near-surface sediments could also be released to the overlying water column via a process known as bio-turbation, or more generally, sediment mixing (e.g., Aller, 1977, 1980). ^{224}Ra flux induced by sediment mixing (F_B) can be expressed as:

$$F_B = D_B \frac{\partial(\phi^{224}Ra_P)}{\partial z} + D_B \frac{\partial[\rho_S(1-\phi)^{224}Ra_S]}{\partial z} \quad (3)$$

where $^{224}Ra_S$ denotes surface-bound ^{224}Ra activity on sediment particles (unit: dpm g^{-1} dry mass); $\frac{\partial[\rho_S(1-\phi)^{224}Ra_S]}{\partial z}$ refers to the concentration gradient of surface-bound ^{224}Ra at the sediment–water interface, which was calculated from total ^{224}Ra measurements in the suspended particles and in the topmost 0–1 cm layer of sediment; D_B represents the sediment mixing coefficient and was estimated from the distribution of $^{234}Th_{ex}$ in the upper sediment column (e.g., Aller and Cochran, 1976). Our calculations showed that during the winter survey, the value of D_B varied from 0.006 ± 0.002 to 0.38 ± 0.13 cm^2 d^{-1} (Table 1). These values bracket our previous estimates in the Yangtze River estuary and the Pearl River estuary (Cai et al., 2014, 2015). With Eq. (3), F_B values were found to fall in the range of -0.43 ± 0.054–0.073 ± 0.006 dpm cm^{-2} d^{-1} dur-

Table 1
Molecular diffusion coefficient of ^{224}Ra in sediments (D_S^{Ra}), sediment mixing coefficient (D_B), observed flux ("+": upward) of ^{224}Ra (F_{Ra}) and theoretical flux of ^{224}Ra induced by molecular diffusion (F_M), sediment mixing (F_B) and irrigation (F_g) in the sediments of the Jiulong River estuary.

Station	D_S^{Ra} ($cm^2\ d^{-1}$)	D_B ($cm^2\ d^{-1}$)	Integrated depth (cm)	F_{Ra} (dpm $cm^{-2}\ d^{-1}$)	F_M (dpm $cm^{-2}\ d^{-1}$)	*F_B (dpm $cm^{-2}\ d^{-1}$)	F_g (dpm $cm^{-2}\ d^{-1}$)
Winter, 2014							
JL0	0.364	0.28 ± 0.11	21	1.17 ± 0.11	0.003 ± 0.002	−0.43 ± 0.054	1.59 ± 0.12
JL1	0.362	0.38 ± 0.13	25	1.25 ± 0.13	0.008 ± 0.002	−0.025 ± 0.069	1.27 ± 0.15
JL2	0.382	0.14 ± 0.038	21	0.400 ± 0.079	0.004 ± 0.002	0.001 ± 0.015	0.40 ± 0.080
JL3	0.306	0.027 ± 0.008	10	0.209 ± 0.082	0.007 ± 0.001	0.052 ± 0.006	0.15 ± 0.082
JL5	0.342	0.031 ± 0.027	15	0.072 ± 0.062	0.037 ± 0.002	0.073 ± 0.006	−0.038 ± 0.062
JL6	0.331	0.046 ± 0.009	10	−0.047 ± 0.036	0.004 ± 0.001	0.026 ± 0.003	−0.076 ± 0.037
JL7	0.354	0.006 ± 0.002	12	0.139 ± 0.023	0.012 ± 0.001	0.006 ± 0.000	0.12 ± 0.023
Summer, 2014							
JL0	0.409	–	10	−0.100 ± 0.088	0.001 ± 0.001	NA	NA
JL1	0.570	–	25	0.891 ± 0.092	0.005 ± 0.002	−0.021 ± 0.050	0.91 ± 0.11
JL2	0.578	–	10	0.137 ± 0.041	0.015 ± 0.003	−0.069 ± 0.007	0.19 ± 0.042
JL3	0.515	–	10	0.138 ± 0.049	0.043 ± 0.004	0.049 ± 0.006	0.046 ± 0.049
JL4	0.570	–	10	0.312 ± 0.041	0.023 ± 0.003	0.071 ± 0.011	0.22 ± 0.043
JL5	0.533	–	10	0.083 ± 0.061	0.038 ± 0.003	0.048 ± 0.004	−0.003 ± 0.061
JL6	0.437	–	25	0.796 ± 0.116	0.026 ± 0.002	0.23 ± 0.050	0.54 ± 0.126
JL7	0.453	–	10	0.107 ± 0.022	0.019 ± 0.003	0.039 ± 0.004	0.048 ± 0.023

NA: Not available because the error associated with the flux calculation was >±100%.
* For the summer survey, values of F_B were calculated using the D_B estimates deduced from the relation of F_{Ra} vs. D_B observed in the winter survey.

ing the winter survey, and of −0.069 ± 0.007–0.23 ± 0.050 dpm $cm^{-2}\ d^{-1}$ during the summer survey. A negative value of F_B could be caused by net absorption of ^{224}Ra from the water column as sediment particles in depth mix to the surface and contact the overlying water. This scenario has been observed in our prior study in the Yangtze River estuary (Cai et al., 2014). It may be a common phenomenon in the upper estuary, where salinity is close to zero and favors net absorption of ^{224}Ra onto sediment particles. Overall, ^{224}Ra fluxes induced by sediment mixing were significantly larger than those induced by molecular diffusion (Table 1). Excluding those locations characterized by low ^{224}Ra fluxes associated with a large uncertainty (i.e., St. JL5 and JL6 in the winter survey, and St. JL0 and JL5 in the summer survey), we found that sediment mixing on average accounted for 14% and 29% of the observed deficit of ^{224}Ra during the winter and summer surveys.

For most of the stations, however, the combination of sediment mixing and molecular diffusion cannot explain the observed deficit of ^{224}Ra in the sediment column. As such, irrigation must be taken into account. Previous studies suggest that in muddy coastal sediments, irrigation generally plays a dominant role in regulating solute transport across the sediment–water interface (e.g., Aller, 2014 and Refs. therein; Cai et al., 2014, 2015). ^{224}Ra flux induced by irrigation (F_g) was thus calculated from the difference between the observed deficit of ^{224}Ra and the flux of ^{224}Ra induced by molecular diffusion plus sediment mixing. Our calculations showed that during the winter and the summer surveys, F_g varied from −0.076 ± 0.037 to 1.59 ± 0.12 dpm $cm^{-2}\ d^{-1}$ and from −0.003 ± 0.061 to 0.91 ± 0.11 dpm $cm^{-2}\ d^{-1}$, respectively (Table 1). At most of the stations, F_g accounted for more than 60% of the observed deficit of ^{224}Ra in the sediment column.

We have identified a strong correlation between the observed deficit of ^{224}Ra and the sediment mixing coefficients for the winter survey ($F_{Ra} = (3.48 \pm 0.42) \times D_B + (0.00 \pm 0.08)$, $R^2 = 0.93$, $P < 0.001$; Fig. 8). While sediment mixing has been demonstrated not to be the dominant process that regulates solute exchange across the sediment–water interface, this strong correlation is consistent with our recognition that sediment mixing (or more specifically, bio-turbation) and irrigation are two inter-correlated processes: benthic organisms mix sediment and the accompanying interstitial waters when they crawl or plow through it – this process is referred to as bio-turbation; in the meantime, benthic organisms construct burrows and tubes within sediment and constantly flush them with overlying seawater – the latter process is known as irrigation (e.g., Berner, 1980). In this regard, Fig. 8 provides strong evidence that the observed deficit of ^{224}Ra in the near-surface sediments within the Jiulong River estuary was indeed induced by small-scale PEX processes, namely bio-turbation and irrigation. Another implication is that $^{234}Th_{ex}$, which was commonly considered as a proxy of sediment mixing, can also be used as an indicator of irrigation. It is interesting to note that the intercept of the relationship between F_{Ra} and D_B is indiscernible from zero. This indicates that other processes, like molecular diffusion, did not exert a significant influence on the benthic fluxes of ^{224}Ra.

4.2. Input of ^{224}Ra from SGD

Input of ^{224}Ra from SGD was assessed by constructing a ^{224}Ra mass balance in the water column. Fig. 9 is a schematic of ^{224}Ra budget in an estuary. Supply terms of ^{224}Ra include riverine discharge (F_{Riv}), desorption from suspended particles (F_{Des}), release via pore water exchange

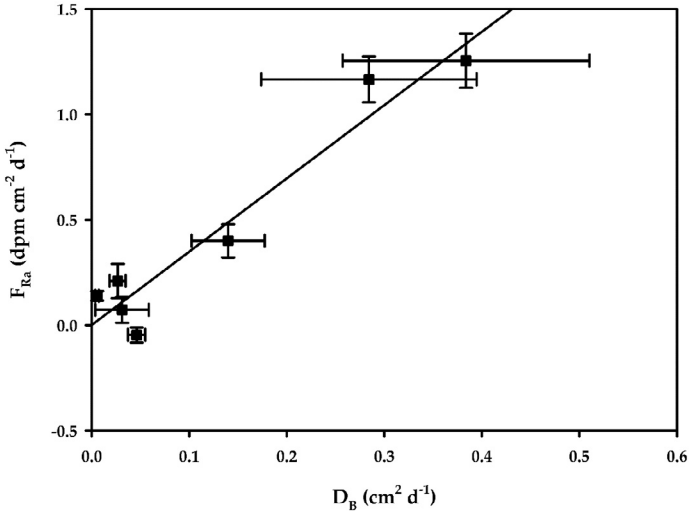

Fig. 8. Correlation of F_{Ra} vs. D_B for the winter survey in 2014.

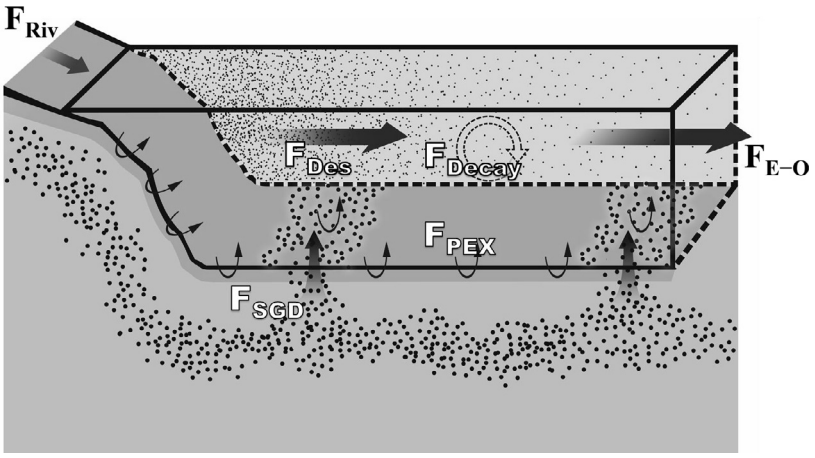

Fig. 9. Schematic diagram of the ^{224}Ra budget in an estuary.

(F_{PEX}), and input from SGD (F_{SGD}). Loss of ^{224}Ra occurs principally via radioactive decay (F_{Decay}) and net export to the adjacent sea (F_{E-O}). Consequently, a mass balance of ^{224}Ra can be set up:

$$F_{Riv} + F_{Des} + F_{PEX} + F_{SGD} = F_{Decay} + F_{E-O} \quad (4)$$

The riverine input of ^{224}Ra (F_{Riv}) was calculated by multiplying the water discharge rate (Q_R) of the river by the activity of ^{224}Ra in the riverine end-member. The mean water discharge rates of the Jiulong River were 250 and 573 $m^3\ s^{-1}$ for the winter and summer surveys, respectively. During the winter survey, no surface water samples with zero salinity were collected. As such, we adopted the ^{224}Ra activity at $S = 0.2$ (1170 ± 32 dpm m^{-3}, see Appendix T2) as the riverine end-member. In the summer survey, ^{224}Ra activities at $S = 0$ spanned over a range of 195 ± 10–665 ± 30 dpm m^{-3}. As such, we took the median of 243 ± 15 dpm m^{-3} as the end-member value. Consequently, for the winter and the summer surveys we yielded a riverine ^{224}Ra input (in 10^{10} dpm d^{-1}) of 2.5 ± 0.64 and 1.2 ± 0.38, respectively (see Table 2).

Desorption rate of ^{224}Ra from suspended particles (F_{Des}) was estimated by directly quantifying the ^{224}Ra deficit in suspended particles and subsequently multiplying the deficit by the concentration of total suspended matter (TSM) (e.g., Cai et al., 2014). In doing so, we placed our measurements into a seven-box grid based on the geometry of the estuary. Box boundaries are shorelines, and demarcations that intersect the axis of the estuary. Consequently, the estuary was divided into seven boxes with an area (S_i) of 1.2, 2.1, 10, 27, 23, 21.5 and 57 km^2, respectively. For the summer survey, the fourth box was further divided into two sub-boxes with an area of 10 and 17 km^2, respectively. Water volume of a specific box was estimated by multiplying the area of the box by the water depth. Desorption rate of ^{224}Ra at each box was added up. In this manner, we estimated that in the Jiulong River estuary, suspended particles supplied ^{224}Ra at a rate of $0.94 \pm 0.06 \times 10^{10}$ dpm d^{-1} during the summer survey. In the winter survey, we did not measure TSM concentration. Under such a circumstance, we used the value derived in the summer survey to construct the ^{224}Ra budget in the winter survey. This should not

Table 2
Notations used in the text and the ^{224}Ra budget in the Jiulong River estuary during the winter and summer, 2014.

Symbol	Description	Winter		Summer	
		Value	Error	Value	Error
λ_{Ra} (d^{-1})	Decay constant of ^{224}Ra	0.189	–	0.189	–
V_E ($\times 10^9$ m^3)	Volume of the estuary	1.62	–	1.62	–
Q_{Riv} (m^3 s^{-1})	Discharge rate of the river	250	63	573	176
τ (d)	Flushing time of the estuary*	2.05	0.95	0.78	0.19
A_{Th}(dpm m^{-3})	Activity of ^{228}Th in suspended particle	2.7	1.1	4.2	1.5
A_{Riv} (dpm m^{-3})	Activity of dissolved ^{224}Ra in the river end-member	1170	32	243	15
A_E (dpm m^{-3})	Volume-weighted average activity of dissolved ^{224}Ra in the estuary	682	95	775	108
A_O (dpm m^{-3})	Activity of dissolved ^{224}Ra in the adjacent sea	478	103	478	103
F_{Riv} ($\times 10^{10}$ dpm d^{-1})	Supply rate of ^{224}Ra via riverine input	2.53	0.64	1.20	0.38
F_{Des} ($\times 10^{10}$ dpm d^{-1})	Desorption rate of ^{224}Ra	0.94	0.06	0.94	0.06
F_{PEX} ($\times 10^{10}$ dpm d^{-1})	Supply rate of ^{224}Ra via pore water exchange	22.3	3.0	33.7	5.5
F_{SGD} ($\times 10^{10}$ dpm d^{-1})	SGD flux of ^{224}Ra	11.3	8.6	49.5	16.3
F_{Decay} ($\times 10^{10}$ dpm d^{-1})	Loss of ^{224}Ra via decay	20.9	2.9	23.7	3.3
$F_{E\text{-}O}$ ($\times 10^{10}$ dpm d^{-1})	Net export flux of ^{224}Ra to the adjacent sea	16.1	7.5	61.6	15.0
R_{SGD} ($\times 10^7$ m^3 d^{-1})	Flow rate of SGD	0.64	0.52	2.83	1.24

* Adopted from Wang et al. (2015).

cause significant bias in the estimation of SGD fluxes given that desorption from suspended particles represents only a small term in the overall budget of ^{224}Ra in the estuary.

The total PEX flux of ^{224}Ra (F_{PEX}) was achieved in a similar fashion. The observed ^{224}Ra flux at each study site was multiplied by the area of the respective box to compute the flux from the sediments. Subsequently, flux of ^{224}Ra from each box was added up. We estimated that pore water exchange supplied ^{224}Ra at a rate (in 10^{10} dpm d^{-1}) of 22.3 ± 3.0 and 33.7 ± 5.5 during the winter and the summer surveys, respectively.

To assess the loss terms in Eq. (4), the average activity of seawater ^{224}Ra (A_E) in the estuary must be known. This value was estimated using the expression $A_E = \frac{\sum(A_i S_i H_i)}{\sum(S_i H_i)}$, where A_i and H_i represent the seawater activity of ^{224}Ra and water depth in a specific box, respectively. Our calculations showed that during the winter and the summer surveys, the volume-weighted average activities of ^{224}Ra were 682 ± 95 dpm m^{-3} and 775 ± 108 dpm m^{-3}, respectively (Table 2). Consequently, the decay term (in 10^{10} dpm d^{-1}) in Eq. (4) was determined to be 20.9 ± 2.9 and 23.7 ± 3.3 for the winter and the summer surveys, respectively. In regard to the second loss term in Eq. (4), i.e., net export of ^{224}Ra out of the estuary (F_{E-O}), it can be estimated using the expression $F_{E-O} = \frac{V_E(A_E - A_O)}{\tau}$, where A_O is the activity of seawater ^{224}Ra in the adjacent sea; τ denotes the water residence time of the estuary. Most recently, Wang et al. (2015) have utilized a tidal prism model to estimate water residence time in the Jiulong River estuary. These investigators derived a value of 2.05 ± 0.95 d during the winter survey, and 0.78 ± 0.19 d during the summer survey. With these estimates, F_{E-O} (in 10^{10} dpm d^{-1}) was calculated to be 16.1 ± 7.5 and 61.6 ± 15.0 for the winter and the summer surveys, respectively.

The source terms detailed above, however, are insufficient to balance the total loss of ^{224}Ra (Table 2). The difference could reasonably be ascribed to deep pore water flow, or submarine groundwater discharge (e.g., Moore et al., 2011). Based on Eq. (4), we estimated that SGD fluxes of ^{224}Ra (in 10^{10} dpm d^{-1}) into the Jiulong River estuary were 11.3 ± 8.6 and 49.5 ± 16.3 for the winter and the summer surveys, respectively. Wang et al. (2015) have recently carried out an extensive survey of SGD around the Jiulong River estuary. Based on the measurements of four brackish groundwater samples ($S > 5$), these investigators identified an average activity of 17,500 ± 5100 dpm m^{-3} for ^{224}Ra in the SGD end-member. With this value, the SGD fluxes of ^{224}Ra were converted to a SGD flow rate (R_{SGD}, in 10^7 m^3 d^{-1}) of 0.64 ± 0.52 (winter survey) and of 2.8 ± 1.2 (summer survey). Notably, Wang et al. (2015) have constructed a mass balance of long-lived ^{226}Ra to estimate SGD flow rates into the Jiulong River estuary. Their results showed that in the winter and summer seasons, SGD flow rates (10^7 m^3 d^{-1}) into the Jiulong River estuary were 0.26–0.54 and 0.69–1.44, respectively. Taking into account the associated uncertainty, our results are in line with these ^{226}Ra-based estimates. Large SGD flow rates in the summer are a response of a greater degree of freshwater intrusion into the aquifer, which in turn is driven by large terrestrial hydraulic gradients set up by high precipitation rates in this season (Wang et al., 2015). In addition, seasonal changes in the aquifer level may also play a role (e.g., Santos et al., 2012).

4.3. Fluxes of DIC and nutrients induced by PEX and SGD

PEX fluxes of DIC and nutrients were assessed using the newly developed ^{224}Ra/^{228}Th disequilibrium approach (Cai et al., 2014, 2015). This approach is based on the observed deficit of ^{224}Ra in the sediment and a general concept of increased sediment surface area for exchange by irrigation. In this model, solute exchange between the sediment and the overlying water is deemed to take place at a highly invaginated interface. In addition, diffusion is assumed to be the rate-limiting step of irrigation, which generally con-

sists of an advection step by which the overlying seawater flushes the burrows in sediment, and a diffusion step by which solutes transfer across the walls of the burrows (Cai et al., 2014, 2015). Consequently, the benthic flux of a dissolved species (F_i) is written as:

$$F_i = F_{Ra}\left(\frac{D_S^i}{D_S^{Ra}}\right)\left(\frac{\frac{\partial C^i}{\partial z}}{\frac{\partial C^{Ra}}{\partial z}}\right) \quad (5)$$

where superscript Ra and i represent ^{224}Ra and the dissolved species i, respectively; $\frac{\partial C}{\partial z}$ denotes the concentration gradient at the interface, and was derived from the measurements in the bottom water and pore water within the topmost 0–1 cm sediment (see Table 3). The uncertainty of F_i was propagated from the errors associated with the ^{224}Ra fluxes and the concentration gradient of dissolved ^{224}Ra at the interface.

PEX fluxes of DIC and nutrients spanned over three orders of magnitude in the Jiulong River estuary (Table 3). As the upper estuary was generally characterized by high ^{224}Ra fluxes, large gradients of DIC and nutrients but small gradients of dissolved ^{224}Ra at the sediment–water interface, it is not surprising that the largest fluxes of DIC and nutrients were usually observed in this region. More specifically, DIC fluxes varied from -6.0 ± 5.1 to 9000 ± 4700 mmol m^{-2} d^{-1} during the winter survey, and from 14 ± 5.0 to $19{,}300 \pm 6400$ mmol m^{-2} d^{-1} during the summer survey. In contrast, fluxes of NO_3^- fell in the range of -530 ± 280–4.4 ± 3.5 mmol m^{-2} d^{-1} during the winter survey, and in the range of -680 ± 230 to -0.4 ± 0.1 mmol m^{-2} d^{-1} during the summer survey. In the respective seasons, NH_4^+ fluxes varied from -2.9 ± 2.3 to 440 ± 230 mmol m^{-2} d^{-1} and from 7.8 ± 5.7 to 870 ± 290 mmol m^{-2} d^{-1}, respectively. Benthic fluxes of H_4SiO_4 changed from -9.9 ± 4.0 to 72 ± 16 mmol m^{-2} d^{-1} in the winter, and from 0.4 ± 0.3 to 190 ± 63 mmol m^{-2} d^{-1} in the summer.

As with the quantification of the total PEX flux of ^{224}Ra, we estimated the total PEX fluxes of DIC and nutrients ($F_{m\text{-}PEX}$) by multiplying the site-specific fluxes by the area of the grid boxes, and subsequently summing up the individual estimates at each box. Our results (in 10^6 mol d^{-1}) showed that the total PEX flux of DIC was 34.6 ± 8.2 and 85.4 ± 14.7 during the winter and the summer surveys, respectively. In the respective seasons, the total PEX flux of NH_4^+ was 2.2 ± 0.40 and 8.8 ± 1.0. In comparison, the total PEX flux of H_4SiO_4 was very similar in the winter and in the summer, approximately 1.4–1.5. Conversely, due to the diagenetic process of denitrification, bottom sediments sequestered NO_3^- from the water column at a rate of 3.4 ± 0.8 during the winter survey, and of 2.3 ± 0.5 during the summer survey. Notably, total PEX fluxes of DIC and NH_4^+ were dramatically larger in the summer compared to the winter. This phenomenon is believed to result from a combination of elevated discharge rates of sediment – hence a higher supply rate of organic matter to the seafloor, and enhanced irrigation rates near the sediment–water interface in the wet season.

In regard to SGD, it includes fresh groundwater and recirculated seawater (Burnett et al., 2003). During the intrusion of estuarine water into the aquifer, solutes are concomitantly carried from the estuary to the subterranean estuary. As such, net export of solutes via SGD should be estimated as the difference between the SGD fluxes and the return fluxes from the estuary into the subterranean estuary, i.e., $F_{m-SGD} = R_{SGD}C_{STE} - R_{SGD}(1-f)C_B$, where C_{STE} is the concentration of solutes in the subterranean estuary (Appendix T3), C_B is the average concentration of solutes in the bottom water, f is the fraction of the fresh groundwater in SGD. A critical assumption associated with this approach is that all the components of the SGD end-member, like ^{224}Ra, DIC, and nutrients, remain constant in its path into the surface estuary. Wang et al. (2015) estimated an f value of 0–54% in winter and 0–47% in summer based on salinity measurements. Tak-

Table 3
Concentration gradient of dissolved ^{224}Ra, DIC, NO_3^-, NH_4^+, and H_4SiO_4 at the sediment–water interface, and benthic fluxes ("+" upward) of DIC, NO_3^-, NH_4^+, and H_4SiO_4 in the Jiulong River estuary in the winter and the summer, 2014.

	$\partial^{224}Ra_p/\partial z$ dpm l^{-1} cm^{-1}	$\partial DIC/\partial z$ mmol l^{-1} cm^{-1}	$\partial NO_3^-/\partial z$ mmol l^{-1} cm^{-1}	$\partial NH_4^+/\partial z$ mmol l^{-1} cm^{-1}	$\partial H_4SiO_4/\partial z$ mmol l^{-1} cm^{-1}	DIC flux mmol m^{-2} d^{-1}	NO_3^- flux mmol m^{-2} d^{-1}	NH_4^+ flux mmol m^{-2} d^{-1}	H_4SiO_4 flux mmol m^{-2} d^{-1}
Winter									
JL0	11.7 ± 6.0	6.8	−0.24	0.19	0.053	9000 ± 4700	-530 ± 280	440 ± 230	64 ± 33
JL1	30.8 ± 6.2	4.0	−0.25	0.24	0.15	2200 ± 490	-230 ± 51	220 ± 50	72 ± 16
JL2	14.3 ± 5.1	3.8	−0.25	0.081	−0.029	1400 ± 570	-160 ± 65	52 ± 21	-9.9 ± 4.0
JL3	36.3 ± 4.9	1.2	−0.15	0.080	0.20	90 ± 37	-19 ± 7.7	10.4 ± 4.3	14 ± 5.8
JL5	149.8 ± 9.7	−0.93	−0.13	0.16	0.35	-6.0 ± 5.1	-1.4 ± 1.2	1.7 ± 1.5	2.1 ± 1.8
JL6	16.1 ± 3.7	−0.082	−0.068	0.044	0.12	3.2 ± 2.6	4.3 ± 3.5	-2.9 ± 2.3	-4.1 ± 3.3
JL7	48.0 ± 5.6	1.3	−0.073	0.12	0.47	50 ± 10	-4.6 ± 0.9	7.9 ± 1.6	17 ± 3.3
Summer									
JL0	2.3 ± 4.3	3.5	−0.22	1.1	0.40	–	–	–	–
JL1	11.2 ± 3.5	18	−0.41	0.50	0.20	$19{,}300 \pm 6400$	-680 ± 230	870 ± 290	190 ± 63
JL2	31.5 ± 5.5	25	−0.27	1.5	0.33	1400 ± 500	-25 ± 8.7	147 ± 51	17 ± 6.3
JL3	112 ± 10.3	0.81	−0.13	0.42	0.046	14 ± 5.0	-3.5 ± 1.3	11 ± 4.2	0.7 ± 0.2
JL4	49.3 ± 6.4	12	−0.17	0.82	0.16	1000 ± 190	-23 ± 4.3	110 ± 21	12 ± 2.2
JL5	92.3 ± 7.7	2.7	−0.11	0.39	0.036	32 ± 24	-2.0 ± 1.5	7.8 ± 5.7	0.4 ± 0.3
JL6	89.0 ± 7.7	6.8	−0.057	0.82	0.21	820 ± 140	-11 ± 1.8	160 ± 28	23 ± 3.9
JL7	59.7 ± 8.1	1.1	−0.010	0.22	0.26	26 ± 6.4	-0.4 ± 0.1	8.8 ± 2.2	5.6 ± 1.4

Table 4
DIC and nutrients fluxes induced by pore water exchange ($F_{m\text{-}PEX}$), submarine groundwater discharge ($F_{m\text{-}SGD}$) and riverine input ($F_{m\text{-}Riv}$) into the Jiulong River estuary in the winter and summer, 2014.

Total flux (10^6 mol d^{-1})	DIC	NO_3^-	NH_4^+	H_4SiO_4
Winter				
$F_{m\text{-}PEX}$	34.6 ± 8.2	-3.4 ± 0.8	2.2 ± 0.4	1.4 ± 0.3
$F_{m\text{-}SGD}$	20.7–27.0	−0.30 to −0.67	1.6–1.8	2.7–3.2
$F_{m\text{-}Riv}$	28.1 ± 7.1	3.5 ± 0.9	4.4 ± 1.1	6.2 ± 1.6
Summer				
$F_{m\text{-}PEX}$	85.4 ± 14.7	-2.3 ± 0.5	8.8 ± 1.0	1.5 ± 0.2
$F_{m\text{-}SGD}$	96.5–118	−1.1 to −2.2	8.4–8.9	13.4–14.4
$F_{m\text{-}Riv}$	39.5 ± 12.1	10.4 ± 3.2	3.5 ± 1.1	12.6 ± 3.9

ing an average DIC concentration of 1788 ± 209 μmol l^{-1} in the bottom water, we estimated that the net SGD flux (in 10^6 mol d^{-1}) of DIC was 20.7–27.0 during the winter survey. In comparison, during the summer survey the net SGD flux of DIC was 96.5–118. The net SGD fluxes of NH_4^+ and H_4SiO_4 were 1.6–1.8 and 2.7–3.2 in the winter, and were 8.4–8.9 and 13.4–14.4 in the summer. In the respective seasons, the net removal rate of NO_3^- via SGD was 0.23–0.67 and 1.1–2.2. To our knowledge, this result represents the first quantification of NO_3^- loss due to SGD. Overall, the net SGD fluxes of solutes in the summer were approximately 5 times higher than those in the winter. It is quite clear that this change is a direct response of the seasonality in the SGD flow rate.

In order to provide a general idea on the significance of PEX and SGD in the overall budget of DIC and nutrients in the Jiulong River estuary, we have compared the total PEX fluxes and SGD fluxes with the riverine inputs of DIC and nutrients (Table 4). Similar to the calculation of the riverine fluxes of ^{224}Ra, we adopted the surface water sample at $S = 0.2$ as the river end-member during the winter survey and the medians of the values at $S = 0$ as the river end-member during the summer survey. We obtained a riverine flux (in 10^6 mol d^{-1}) of 28 ± 7.1 for DIC, of 3.5 ± 0.9 for NO_3^-, of 4.4 ± 1.1 for NH_4^+, and 6.2 ± 1.6 for H_4SiO_4 in the winter survey. In comparison, in the summer survey the riverine inputs of DIC, NO_3^-, NH_4^+, and H_4SiO_4 were 39.5 ± 12.1, 10.4 ± 3.2, 3.5 ± 1.1, and 12.6 ± 3.9, respectively. As showed in Table 4, the total PEX fluxes and SGD fluxes of DIC and NH_4^+ were generally comparable or significantly higher than the riverine inputs. This comparison highlights the importance of bottom sediments and SGD as pronounced sources of DIC, NH_4^+, and H_4SiO_4 in the Jiulong River estuary. It also revealed that bottom sediments and SGD are strong sinks of NO_3^- during estuarine mixing.

5. CONCLUDING REMARKS

The utilization of the radium quartet as a proxy of submarine groundwater discharge (SGD) generally involves the construction of mass balances of the isotopes in the water column. Therefore, accurate constraint of all the supply terms and loss terms other than SGD is critically important for the successful application of the radium approach. Historical SGD studies based on the short-lived ^{224}Ra and ^{223}Ra, however, had been jeopardized by our inability to tightly constrain their rapid regeneration rates in bottom sediments. In this study, we have pursued the recently developed $^{224}Ra/^{228}Th$ disequilibrium approach to acquire benthic fluxes of ^{224}Ra in a coastal setting – the Jiulong River estuary. Compared to the traditional incubation method, the $^{224}Ra/^{228}Th$ disequilibrium approach offers a higher sampling resolution and the most reliable flux estimates of ^{224}Ra. This is particularly important for ^{224}Ra-based SGD studies in the coastal seas, where bottom sediments are generally highly heterogeneous and flow fields are very dynamic. By constructing a full mass balance of water column ^{224}Ra, we were allowed to put various source terms, i.e., SGD, PEX-driven flux, and river input in a single context. This led to the first quantitative assessment of the relative importance of PEX vs. SGD in the delivery of solutes into an estuary. We demonstrated that the PEX-driven fluxes of ^{224}Ra, DIC and nutrients were comparable in magnitude to the concomitant fluxes of SGD. Instead of being a type of SGD, which is generally considered as a source of "new" materials, PEX should be viewed as a separate pathway for the regenerated components of benthic respiration. As such, unambiguous discrimination of PEX and SGD components will help to better understand how an ecosystem functions in the coastal ocean. It also has clear significance for water quality management. In this aspect, our study provides a general approach of assessing the relative importance of inputs from autochthonous vs. allochthonous components into a coastal system.

ACKNOWLEDGEMENT

We thank Lingfeng Liu for his help in sample collection, and the crew on R/V Ocean II for their assistance in the cruises. Thanks are also due to the associate editor, Claudine Stirling, as well as M. M. Rutgers van der Loeff, and an anonymous reviewer for their constructive comments on an earlier version of this manuscript. This work was supported by the Natural Science Foundation of China (NSFC) through Grants No. 41576072 and 41276062, and by the National Major Scientific Research Project of China through Grants No. 2015CB954003 and 2016YFC0300709. Support of this work also came from the National Basic Research Program ("973" program) of China (Grant No. 2014CB953702).

APPENDIX T1-T3

Appendix T1
Porosity, DIC, nutrients and ^{224}Ra ($^{224}Ra_P$) in pore water, as well as total ^{224}Ra ($^{224}Ra_T$), ^{228}Th and $^{234}Th_{ex}$ activities in the near-surface sediments of the Jiulong River estuary.

Depth (cm)	Porosity (ϕ)	DIC (μmol l^{-1})	NO_3^- (μmol l^{-1})	NH_4^+ (μmol l^{-1})	H_4SiO_4 (μmol l^{-1})	$^{224}Ra_P$ (dpm l^{-1})	$^{224}Ra_T$ (dpm g^{-1})	^{228}Th (dpm g^{-1})	$^{224}Ra/^{228}Th$ (A. R.)	$^{234}Th_{ex}$ (dpm g^{-1})
Winter, 2014										
Station: JL0; 24.4650°N, 117.8011°E; Depth = 4.8 m; $T = 14.2$ °C; $S = 0.0$;										
Bottom water	–	1416	161	190	275	0.48 ± 0.03	4.69 ± 0.12	4.70 ± 0.11	1.00 ± 0.03	–
0–0.5	0.822	4802	41	286	301	6.3 ± 3.0	2.39 ± 0.07	3.16 ± 0.09	0.76 ± 0.03	0.78 ± 0.11
0.5–1	0.722									0.89 ± 0.09
1–2	0.723	6932	11.4	310	366	10.2 ± 2.5	4.31 ± 0.12	5.55 ± 0.14	0.78 ± 0.03	1.28 ± 0.11
2–3	0.803	7440	2.9	405	399	16.7 ± 3.0	5.03 ± 0.14	6.18 ± 0.16	0.81 ± 0.03	2.06 ± 0.15
3–4	0.806	9256	0.9	554	428	10.9 ± 3.2	4.37 ± 0.12	4.80 ± 0.13	0.91 ± 0.04	0.56 ± 0.09
4–5	0.812	9529	1.3	634	450	14.3 ± 3.4	4.14 ± 0.11	4.89 ± 0.13	0.85 ± 0.03	0.63 ± 0.09
5–6	0.808	10,000	0.8	587	471	19.8 ± 4.2	4.10 ± 0.12	4.85 ± 0.13	0.84 ± 0.03	1.19 ± 0.11
7–8	0.808	10,320	0.3	477	426	10.4 ± 2.9	3.93 ± 0.12	3.97 ± 0.11	0.99 ± 0.04	0.45 ± 0.08
9–10	0.779	10,820	0.0	532	397	11.6 ± 2.4	4.52 ± 0.13	4.80 ± 0.12	0.94 ± 0.04	−0.01 ± 0.08
11–12	0.773	11,990	0.3	737	387	9.4 ± 2.8	5.54 ± 0.16	6.03 ± 0.16	0.92 ± 0.04	ND
14–15	0.712	12,780	3.3	860	373	11.5 ± 2.7	3.84 ± 0.11	4.44 ± 0.12	0.86 ± 0.03	ND
17–18	–	–	–	–	–	–	4.46 ± 0.13	4.78 ± 0.13	0.93 ± 0.04	ND
20–21	–	–	–	–	–	–	5.32 ± 0.15	5.06 ± 0.14	1.05 ± 0.04	ND
Station: JL1; 24.4196°N, 117.8684°E; Depth = 3.0 m; $T = 16.2$ °C; $S = 2.4$;										
Bottom water	–	1709	145	153	184	1.6 ± 0.06	2.85 ± 0.07	3.51 ± 0.08	0.81 ± 0.03	–
0–0.5	0.777	3706	19	273	273	17.0 ± 3.1	2.52 ± 0.08	3.39 ± 0.09	0.74 ± 0.03	0.83 ± 0.10
0.5–1	0.731									0.38 ± 0.08
1–2	0.722	4644	2.4	387	284	18.9 ± 2.9	3.38 ± 0.09	4.04 ± 0.10	0.84 ± 0.03	0.49 ± 0.08
2–3	0.818	5958	1.3	476	299	21.5 ± 3.6	3.70 ± 0.11	4.46 ± 0.12	0.83 ± 0.03	0.43 ± 0.07
3–4	0.707	7071	1.5	582	316	19.5 ± 3.9	4.33 ± 0.12	4.79 ± 0.13	0.90 ± 0.03	0.25 ± 0.07
4–5	0.655	7781	0.4	749	334	25.5 ± 3.6	2.82 ± 0.08	3.14 ± 0.08	0.90 ± 0.03	0.61 ± 0.08
5–6	0.771	8969	6.4	659	343	19.4 ± 4.3	3.29 ± 0.09	3.44 ± 0.09	0.96 ± 0.04	0.38 ± 0.08
7–8	0.755	11,550	0.7	768	353	19.0 ± 3.1	4.35 ± 0.13	4.84 ± 0.13	0.90 ± 0.04	0.49 ± 0.08
9–10	0.743	12,930	0.0	800	366	17.8 ± 2.7	3.20 ± 0.09	3.53 ± 0.09	0.91 ± 0.03	0.01 ± 0.08
11–12	0.751	13,310	0.1	1040	351	17.5 ± 3.8	3.24 ± 0.10	3.64 ± 0.10	0.89 ± 0.04	ND
14–15	0.728	12,090	0.0	1220	362	19.4 ± 3.0	3.36 ± 0.10	3.92 ± 0.11	0.86 ± 0.04	ND
18–19	–	–	–	–	–	–	3.57 ± 0.11	3.89 ± 0.11	0.92 ± 0.04	ND
24–25	–	–	–	–	–	–	4.54 ± 0.13	4.51 ± 0.12	1.01 ± 0.04	ND
Station: JL2; 24.4138°N, 117.8783°E; Depth = 4.2 m; $T = 14.0$ °C; $S = 6.3$;										
Bottom water	–	1669	149	151	199	1.7 ± 0.06	2.32 ± 0.06	3.03 ± 0.07	0.77 ± 0.03	–
0–0.5	0.830	3549	21	191	184	8.8 ± 2.6	2.29 ± 0.06	2.95 ± 0.07	0.78 ± 0.03	1.42 ± 0.12
0.5–1	0.824									1.33 ± 0.12
1–2	0.843	4103	7.4	239	207	19.3 ± 2.9	3.86 ± 0.10	4.47 ± 0.11	0.86 ± 0.03	1.12 ± 0.11
2–3	0.805	5482	3.1	309	216	21.8 ± 3.5	3.76 ± 0.10	4.02 ± 0.10	0.94 ± 0.03	0.85 ± 0.09
3–4	0.828	6729	2.9	340	214	17.3 ± 3.4	3.40 ± 0.09	3.43 ± 0.09	0.99 ± 0.04	1.38 ± 0.12

4–5	0.825	7270	2.5	391	231	27.2 ± 3.5	3.26 ± 0.09	3.80 ± 0.10	0.86 ± 0.03	0.72 ± 0.09
5–6	0.826	8792	2.5	431	259	16.2 ± 3.5	3.11 ± 0.08	3.37 ± 0.08	0.92 ± 0.03	0.72 ± 0.09
7–8	0.819	10,720	1.1	484	304	19.1 ± 2.6	3.12 ± 0.10	3.35 ± 0.10	0.93 ± 0.04	0.94 ± 0.09
9–10	0.791	12,810	1.5	724	335	27.8 ± 3.1	4.47 ± 0.12	4.63 ± 0.12	0.97 ± 0.04	0.00 ± 0.09
11–12	0.747	15,730	2.0	935	354	34.1 ± 4.3	4.68 ± 0.13	4.55 ± 0.12	1.03 ± 0.04	ND
14–15	0.765	19,340	1.1	1210	367	35.2 ± 3.6	3.84 ± 0.11	4.10 ± 0.11	0.94 ± 0.04	ND
17–18	–	–	–	–	–	–	3.80 ± 0.11	3.74 ± 0.10	1.02 ± 0.04	ND
20–21	–	–	–	–	–	–	2.86 ± 0.08	3.20 ± 0.08	0.89 ± 0.03	ND
Station: JL3; 24.3987°N, 117.9179°E; Depth = 5.7 m; T = 15.4 °C; S = 21.5;										
Bottom water	–	1819	107	57	100	0.88 ± 0.04	1.16 ± 0.06	1.82 ± 0.07	0.64 ± 0.04	–
0–0.5	0.681	2406	33	96	202	19.0 ± 2.4	2.29 ± 0.07	2.76 ± 0.08	0.83 ± 0.03	1.15 ± 0.10
0.5–1	0.665									0.48 ± 0.08
1–2	0.687	3339	9.4	125	235	48.9 ± 4.5	3.15 ± 0.09	3.27 ± 0.09	0.96 ± 0.04	0.62 ± 0.08
2–3	0.621	3424	4.7	218	289	57.4 ± 4.5	4.17 ± 0.11	4.39 ± 0.12	0.95 ± 0.04	0.15 ± 0.06
3–4	0.638	3428	4.5	259	294	77.2 ± 6.1	5.25 ± 0.14	5.63 ± 0.15	0.93 ± 0.04	0.06 ± 0.08
4–5	0.645	4734	5.8	347	304	89.2 ± 6.2	6.01 ± 0.16	6.02 ± 0.16	1.00 ± 0.04	0.02 ± 0.07
5–6	0.700	5431	3.8	557	333	64.7 ± 5.9	4.86 ± 0.14	4.79 ± 0.14	1.01 ± 0.04	0.00 ± 0.09
7–8	0.656	6910	1.0	724	354	63.4 ± 5.7	4.95 ± 0.14	4.59 ± 0.13	1.08 ± 0.04	0.19 ± 0.07
9–10	0.655	7768	0.3	815	403	56.2 ± 4.0	4.22 ± 0.13	4.80 ± 0.13	0.88 ± 0.04	0.77 ± 0.09
11–12	0.686	9611	0.5	967	389	51.0 ± 4.3	4.96 ± 0.14	4.99 ± 0.14	0.99 ± 0.04	ND
14–15	0.564	11,600	3.1	1180	401	63.8 ± 5.3	4.65 ± 0.13	4.49 ± 0.13	1.04 ± 0.04	ND
Station: JL5; 24.4259°N, 117.9704°E; Depth = 8.0 m; T = 14.7 °C; S = 23.7;										
Bottom water	–	1923	79	25	66	0.92 ± 0.04	1.19 ± 0.05	2.47 ± 0.07	0.48 ± 0.02	–
0–0.5	0.747	1457	14	103	242	75.8 ± 4.8	2.99 ± 0.09	2.94 ± 0.08	1.02 ± 0.04	0.65 ± 0.09
0.5–1	0.750									0.12 ± 0.08
1–2	0.743	1087	3.5	167	403	119 ± 8.1	3.52 ± 0.10	3.94 ± 0.10	0.89 ± 0.03	0.53 ± 0.09
2–3	0.729	1396	2.7	229	451	82.1 ± 5.7	3.96 ± 0.11	3.90 ± 0.10	1.01 ± 0.04	0.75 ± 0.10
3–4	0.733	1983	3.2	239	461	102 ± 7.0	3.73 ± 0.10	3.51 ± 0.09	1.06 ± 0.04	0.01 ± 0.09
4–5	0.733	2245	4.6	305	445	99.6 ± 7.2	3.75 ± 0.10	3.49 ± 0.09	1.07 ± 0.04	0.44 ± 0.10
5–6	0.730	2388	1.4	310	399	99.8 ± 7.1	2.99 ± 0.09	3.00 ± 0.08	1.00 ± 0.04	0.02 ± 0.09
7–8	0.736	4250	2.8	382	412	79.8 ± 5.9	2.85 ± 0.08	2.91 ± 0.08	0.98 ± 0.04	0.61 ± 0.09
9–10	0.739	4851	0.8	449	397	62.8 ± 4.3	3.23 ± 0.10	3.38 ± 0.09	0.96 ± 0.04	ND
11–12	0.732	6161	2.2	528	404	69.5 ± 4.9	3.25 ± 0.10	3.38 ± 0.09	0.96 ± 0.04	ND
14–15	0.686	6962	3.6	594	391	81.5 ± 6.6	2.45 ± 0.07	2.45 ± 0.06	1.00 ± 0.04	ND
Station: JL6; 24.4267°N, 118.0174°E; Depth = 14.0 m; T = 16.3 °C; S = 27.4;										
Bottom water	–	1961	67	16	54	0.78 ± 0.03	1.13 ± 0.03	2.07 ± 0.04	0.55 ± 0.02	–
0–0.5	0.846	1920	33	38	112	8.8 ± 1.8	1.64 ± 0.04	1.68 ± 0.04	0.97 ± 0.04	2.86 ± 0.20
0.5–1	0.809									1.84 ± 0.14
1–2	0.760	2283	8.0	99	141	12.6 ± 2.5	2.66 ± 0.07	2.50 ± 0.07	1.06 ± 0.04	0.92 ± 0.09
2–3	0.792	2317	3.6	108	163	14.2 ± 2.5	2.70 ± 0.07	2.70 ± 0.07	1.00 ± 0.04	0.55 ± 0.07
3–4	0.730	2905	3.7	136	180	17.3 ± 3.3	2.59 ± 0.07	2.55 ± 0.07	1.02 ± 0.04	0.70 ± 0.07
4–5	0.675	2602	4.2	123	188	56.9 ± 4.6	2.84 ± 0.07	2.54 ± 0.06	1.12 ± 0.04	0.09 ± 0.06

5–6	0.629	2868	5.4	138	208	41.5 ± 4.6	2.27 ± 0.06	2.21 ± 0.06	1.03 ± 0.04	ND
7–8	0.594	2902	0.9	140	225	36.3 ± 3.3	1.98 ± 0.05	2.06 ± 0.05	0.96 ± 0.04	ND
9–10	0.543	2705	4.7	162	262	39.9 ± 3.6	1.82 ± 0.05	1.83 ± 0.05	0.99 ± 0.04	ND
11–12	0.553	2804	3.6	165	275	54.1 ± 4.8	1.41 ± 0.04	1.44 ± 0.04	0.98 ± 0.04	ND
14–15	0.628	2493	1.2	190	300	56.0 ± 4.2	1.38 ± 0.04	1.31 ± 0.03	1.05 ± 0.04	ND
Station: JL7; 24.4059°N, 118.1060°E; Depth = 16.2 m; T = 16.7 °C; S = 29.0;										
Bottom water	–	2021	43	3.6	35	0.41 ± 0.02	0.58 ± 0.03	1.38 ± 0.04	0.42 ± 0.02	–
0–0.5	0.754	2669	6.7	64	271	24.4 ± 2.8	1.36 ± 0.04	1.41 ± 0.04	0.97 ± 0.04	1.28 ± 0.10
0.5–1	0.727									0.34 ± 0.06
1–2	0.707	2549	6.1	86	339	42.0 ± 5.1	1.35 ± 0.04	1.38 ± 0.04	0.98 ± 0.04	0.22 ± 0.05
2–3	0.702	2656	5.6	131	382	38.2 ± 4.0	1.70 ± 0.04	1.85 ± 0.05	0.92 ± 0.03	0.36 ± 0.06
3–4	0.729	3635	4.4	160	402	44.1 ± 4.4	1.29 ± 0.04	1.40 ± 0.04	0.92 ± 0.03	0.00 ± 0.06
4–5	0.721	3706	3.5	192	408	36.7 ± 4.5	1.28 ± 0.03	1.41 ± 0.04	0.90 ± 0.03	0.01 ± 0.05
5–6	0.677	4566	3.0	262	409	34.2 ± 3.9	1.29 ± 0.04	1.33 ± 0.04	0.97 ± 0.04	0.16 ± 0.05
7–8	0.748	5358	1.8	352	432	39.8 ± 4.2	1.21 ± 0.04	1.35 ± 0.04	0.90 ± 0.04	0.29 ± 0.05
9–10	0.723	5985	2.1	557	407	31.5 ± 3.3	1.53 ± 0.04	1.62 ± 0.04	0.94 ± 0.04	ND
11–12	0.709	6877	3.4	596	437	35.2 ± 3.4	1.22 ± 0.04	1.24 ± 0.03	0.99 ± 0.04	ND
14–15	0.733	8072	1.4	667	492	34.8 ± 4.3	1.34 ± 0.04	1.35 ± 0.04	0.99 ± 0.04	ND
Summer, 2014										
Station: JL0; 24.4603°N, 117.8060°E; Depth = 9.4 m; T = 29.6 °C; S = 0.0; *TSM = 101 mg l^{-1}										
Bottom water	–	956	214	138	140	0.26 ± 0.02	8.01 ± 0.21	6.41 ± 0.18	1.25 ± 0.05	–
0–0.5	0.498	2682	105	680	342	1.4 ± 2.1	1.65 ± 0.07	1.59 ± 0.07	1.04 ± 0.06	ND
0.5–1	0.572									ND
1–2	0.623	3904	61	1430	373	1.1 ± 2.0	3.83 ± 0.11	3.75 ± 0.10	1.02 ± 0.04	ND
2–3	0.636	6053	77	2280	396	4.2 ± 2.8	5.13 ± 0.16	4.84 ± 0.14	1.06 ± 0.05	ND
3–4	0.632	7671	51	1740	348	–	4.31 ± 0.13	4.37 ± 0.12	0.99 ± 0.04	ND
4–5	0.655	9320	16	2970	498	8.7 ± 3.1	4.58 ± 0.13	4.36 ± 0.12	1.05 ± 0.04	ND
5–6	0.667	11,010	23	3090	497	5.3 ± 2.8	4.97 ± 0.16	5.09 ± 0.14	0.98 ± 0.04	ND
7–8	0.682	13,510	9.0	3460	496	11.2 ± 2.4	5.45 ± 0.16	5.43 ± 0.14	1.00 ± 0.04	ND
9–10	0.677	15,420	7.9	3850	188	7.5 ± 2.3	5.28 ± 0.16	5.22 ± 0.15	1.01 ± 0.04	ND
11–12	0.690	17,650	8.4	4520	213	13.8 ± 3.3	4.99 ± 0.17	4.83 ± 0.16	1.03 ± 0.05	ND
14–15	0.703	18,160	9.8	4390	211	16.9 ± 3.1	5.12 ± 0.15	4.92 ± 0.14	1.04 ± 0.04	ND
18–19	0.505	–	–	–	–	–	3.81 ± 0.12	3.86 ± 0.12	0.99 ± 0.04	ND
Station: JL1; 24.4261°N, 117.8537°E; Depth = 5.5 m; T = 29.7 °C; S = 0; *TSM = 190 mg l^{-1}										
Bottom water	–	850	221	111	100	0.22 ± 0.02	6.08 ± 0.15	5.59 ± 0.14	1.09 ± 0.04	–
0–0.5	0.863	9901	15	360	201	5.8 ± 1.8	5.70 ± 0.16	7.13 ± 0.18	0.80 ± 0.03	ND
0.5–1	0.848									ND
1–2	0.837	13,440	2.5	485	301	2.5 ± 1.5	4.71 ± 0.13	5.47 ± 0.13	0.86 ± 0.03	ND
2–3	0.826	14,730	1.6	566	293	–	4.02 ± 0.11	4.62 ± 0.12	0.87 ± 0.03	ND
3–4	0.818	17,060	1.7	757	308	–	4.30 ± 0.12	4.41 ± 0.12	0.97 ± 0.04	ND
4–5	0.817	18,220	1.8	735	264	4.1 ± 1.8	3.91 ± 0.11	4.28 ± 0.11	0.91 ± 0.03	ND
5–6	0.815	19,070	1.3	914	252	4.0 ± 1.8	4.15 ± 0.12	4.51 ± 0.12	0.92 ± 0.04	ND

7–8	0.814	20,160	2.2	996	315	7.1 ± 1.8	4.09 ± 0.11	4.51 ± 0.11	0.91 ± 0.03	ND
9–10	0.813	21,470	1.8	1170	362	5.0 ± 1.6	4.24 ± 0.13	4.73 ± 0.13	0.90 ± 0.04	ND
11–12	0.809	21,500	8.1	1330	–	8.1 ± 2.2	4.37 ± 0.10	5.00 ± 0.10	0.87 ± 0.03	ND
14–15	0.807	22,160	1.5	1410	247	6.8 ± 1.9	4.03 ± 0.11	4.49 ± 0.11	0.90 ± 0.03	ND
18–19	–	–	–	–	–	–	3.77 ± 0.10	4.02 ± 0.11	0.94 ± 0.04	ND
24–25	–	–	–	–	–	–	4.13 ± 0.11	3.93 ± 0.10	1.05 ± 0.04	ND
Station: JL2; 24.4141°N, 117.8537°E; Depth = 5.4 m; T = 30.4 °C; S = 0.0; *TSM = 379 mg l^{-1}										
Bottom water	–	907	177	104	128	0.36 ± 0.02	5.37 ± 0.14	5.25 ± 0.13	1.02 ± 0.04	–
0–0.5	0.839	13,230	41	865	292	16.1 ± 2.8	3.16 ± 0.08	3.25 ± 0.08	0.97 ± 0.04	ND
0.5–1	0.828									ND
1–2	0.812	18,470	28	1160	48	14.3 ± 2.8	5.09 ± 0.13	5.70 ± 0.14	0.89 ± 0.03	ND
2–3	0.809	18,940	14	1340	52	9.8 ± 2.7	4.58 ± 0.13	4.97 ± 0.13	0.92 ± 0.03	ND
3–4	0.828	18,330	12	1220	55	9.8 ± 2.5	4.98 ± 0.10	4.73 ± 0.10	1.05 ± 0.03	ND
4–5	0.829	18,560	8.0	1200	78	20.7 ± 3.2	4.96 ± 0.13	5.00 ± 0.13	0.99 ± 0.04	ND
5–6	0.829	18,830	7.7	1240	84	16.6 ± 2.9	5.28 ± 0.14	5.45 ± 0.13	0.97 ± 0.04	ND
7–8	0.826	18,580	7.6	1240	72	21.4 ± 2.7	5.30 ± 0.14	5.35 ± 0.13	0.99 ± 0.04	ND
9–10	0.827	18,720	7.3	1290	71	14.7 ± 2.2	4.72 ± 0.13	4.99 ± 0.13	0.95 ± 0.04	ND
11–12	0.824	18,930	6.9	1300	104	21.9 ± 3.1	4.66 ± 0.10	4.59 ± 0.09	1.02 ± 0.03	ND
14–15	0.809	20,070	13	1250	97	19.1 ± 2.8	4.85 ± 0.13	4.73 ± 0.12	1.03 ± 0.04	ND
18–19	–	–	–	–	–	–	3.71 ± 0.11	3.80 ± 0.10	0.98 ± 0.04	ND
24–25	–	–	–	–	–	–	4.32 ± 0.12	4.46 ± 0.11	0.97 ± 0.04	ND
Station: JL3; 24.3992°N, 117.9179°E; Depth = 5.4 m; T = 31.3 °C; S = 20.5; *TSM = 31 mg l^{-1}										
Bottom water	–	1667	75	23	96	0.68 ± 0.03	2.54 ± 0.09	3.61 ± 0.11	0.70 ± 0.03	–
0–0.5	0.817	2074	7.5	231	119	56.6 ± 5.1	3.47 ± 0.09	4.31 ± 0.11	0.81 ± 0.03	ND
0.5–1	0.775									ND
1–2	0.793	2210	2.0	228	123	50.9 ± 4.4	4.82 ± 0.13	4.78 ± 0.13	1.01 ± 0.04	ND
2–3	0.769	2380	2.0	288	123	70.3 ± 5.4	4.14 ± 0.11	4.01 ± 0.10	1.03 ± 0.04	ND
3–4	0.725	2672	2.8	291	129	51.5 ± 4.3	3.62 ± 0.10	3.67 ± 0.10	0.98 ± 0.04	ND
4–5	0.758	3411	1.8	345	100	64.9 ± 4.6	4.40 ± 0.13	4.44 ± 0.12	0.99 ± 0.04	ND
5–6	0.748	3900	1.4	433	178	46.7 ± 3.8	3.95 ± 0.11	3.90 ± 0.10	1.01 ± 0.04	ND
7–8	0.729	4934	1.0	538	96	35.0 ± 4.0	3.74 ± 0.11	3.87 ± 0.10	0.97 ± 0.04	ND
9–10	0.691	4898	1.1	605	123	24.5 ± 4.0	2.70 ± 0.07	2.64 ± 0.07	1.02 ± 0.04	ND
11–12	0.725	5108	1.3	723	150	39.4 ± 4.8	4.78 ± 0.13	4.90 ± 0.12	0.98 ± 0.04	ND
14–15	0.687	5669	2.1	706	137	39.5 ± 6.1	3.67 ± 0.10	3.70 ± 0.10	0.99 ± 0.04	ND
18–19	–	–	–	–	–	–	3.28 ± 0.09	3.14 ± 0.08	1.04 ± 0.04	ND
24–25	–	–	–	–	–	–	2.79 ± 0.08	2.92 ± 0.07	0.96 ± 0.04	ND
Station: JL4; 24.4010°N, 117.9072°E; Depth = 7.4 m; T = 30.8 °C; S = 14.8; *TSM = 31 mg l^{-1}										
Bottom water	–	1532	96	28	126	0.80 ± 0.03	2.24 ± 0.08	3.86 ± 0.11	0.58 ± 0.03	–
0–0.5	0.839	7572	9.0	437	204	25.5 ± 3.2	3.17 ± 0.08	4.11 ± 0.10	0.77 ± 0.03	ND
0.5–1	0.835									ND
1–2	0.821	11,150	3.2	533	209	26.4 ± 3.1	3.95 ± 0.10	4.40 ± 0.11	0.90 ± 0.03	ND
2–3	0.757	16,250	1.6	549	240	25.1 ± 3.4	4.98 ± 0.15	5.62 ± 0.12	0.89 ± 0.03	ND

3–4	0.785	18,670	1.3	581	232	33.6 ± 4.1	3.54 ± 0.09	4.12 ± 0.10	0.86 ± 0.03	ND
4–5	0.827	20,730	2.8	706	242	47.6 ± 4.6	3.65 ± 0.09	3.94 ± 0.10	0.93 ± 0.03	ND
5–6	0.833	22,580	2.3	686	315	45.1 ± 4.6	3.83 ± 0.10	3.96 ± 0.10	0.97 ± 0.03	ND
7–8	0.819	26,130	0.81	844	372	20.9 ± 2.7	4.79 ± 0.13	4.67 ± 0.11	1.03 ± 0.04	ND
9–10	0.786	28,220	0.79	887	272	21.5 ± 2.7	5.59 ± 0.15	5.63 ± 0.13	0.99 ± 0.04	ND
11–12	0.821	29,690	0.82	1010	337	25.0 ± 4.0	5.02 ± 0.16	5.01 ± 0.12	1.00 ± 0.04	ND
14–15	0.803	30,560	1.7	935	274	34.8 ± 3.7	5.32 ± 0.15	5.16 ± 0.13	1.03 ± 0.04	ND
18–19	–	–	–	–	–	–	5.64 ± 0.16	5.60 ± 0.13	1.01 ± 0.04	ND
24–25	–	–	–	–	–	–	5.32 ± 0.14	5.22 ± 0.12	1.02 ± 0.04	ND
Station: JL5; 24.4035°N, 117.9457°E; Depth = 8.3 m; $T = 31.2$ °C; $S = 22.7$; *TSM = 40 mg l^{-1}										
Bottom water	–	1762	57	21	76	0.69 ± 0.03	2.12 ± 0.08	3.76 ± 0.11	0.56 ± 0.03	–
0–0.5	0.816	3088	4.6	217	95	46.8 ± 3.8	3.83 ± 0.11	4.58 ± 0.12	0.84 ± 0.03	ND
0.5–1	0.774									ND
1–2	0.790	5105	2.7	544	111	87.4 ± 5.0	5.71 ± 0.16	5.71 ± 0.15	1.00 ± 0.04	ND
2–3	0.793	6792	2.6	904	191	106 ± 6.4	5.32 ± 0.15	5.32 ± 0.14	1.00 ± 0.04	ND
3–4	0.786	8186	1.0	855	210	99.3 ± 6.1	5.52 ± 0.15	5.38 ± 0.14	1.03 ± 0.04	ND
4–5	0.780	11,140	2.4	1590	222	108 ± 5.5	4.43 ± 0.10	4.45 ± 0.10	0.99 ± 0.03	ND
5–6	0.787	13,190	1.5	2000	199	91.5 ± 4.7	5.18 ± 0.14	5.08 ± 0.13	1.02 ± 0.04	ND
7–8	0.763	18,280	1.1	2490	183	82.2 ± 4.8	5.89 ± 0.17	5.92 ± 0.15	1.00 ± 0.04	ND
9–10	0.768	19,610	0.88	2530	178	52.0 ± 4.4	6.04 ± 0.17	5.96 ± 0.15	1.01 ± 0.04	ND
11–12	0.644	19,170	0.59	2600	165	58.0 ± 4.1	4.78 ± 0.14	4.32 ± 0.11	1.11 ± 0.04	ND
14–15	0.765	20,940	0.55	2640	206	55.4 ± 4.1	4.67 ± 0.14	4.71 ± 0.12	0.99 ± 0.04	ND
18–19	0.740	–	–	–	–	–	5.02 ± 0.17	5.00 ± 0.15	1.00 ± 0.04	ND
24–25	–	–	–	–	–	–	3.70 ± 0.11	3.67 ± 0.10	1.01 ± 0.04	ND
Station: JL6; 24.4291°N, 118.0131°E; Depth = 12.7 m; $T = 28.6$ °C; $S = 25.1$; *TSM = 46 mg l^{-1}										
Bottom Water	–	1879	37	13	43	0.76 ± 0.03	2.37 ± 0.07	3.28 ± 0.08	0.72 ± 0.03	–
0–0.5	0.674	5289	8.0	421	148	45.2 ± 3.9	2.74 ± 0.08	3.00 ± 0.08	0.92 ± 0.03	ND
0.5–1	0.623									ND
1–2	0.599	6419	2.6	676	123	45.4 ± 3.4	3.02 ± 0.08	2.86 ± 0.08	1.06 ± 0.04	ND
2–3	0.663	7152	1.8	669	117	97.9 ± 5.9	3.17 ± 0.09	3.13 ± 0.09	1.01 ± 0.04	ND
3–4	0.698	7048	2.8	759	166	77.4 ± 4.8	3.33 ± 0.10	3.85 ± 0.10	0.87 ± 0.03	ND
4–5	0.696	7660	1.4	813	168	97.4 ± 5.6	3.74 ± 0.11	4.47 ± 0.12	0.84 ± 0.03	ND
5–6	0.747	7628	1.2	821	182	81.9 ± 4.6	3.71 ± 0.10	4.06 ± 0.11	0.91 ± 0.03	ND
7–8	0.766	7360	1.0	801	217	71.1 ± 4.4	3.77 ± 0.11	4.51 ± 0.11	0.84 ± 0.03	ND
9–10	0.746	8296	0.56	882	218	67.6 ± 5.1	3.99 ± 0.11	3.86 ± 0.10	1.03 ± 0.04	ND
11–12	0.716	7003	0.99	679	173	73.3 ± 5.1	3.66 ± 0.10	3.33 ± 0.09	1.10 ± 0.04	ND
14–15	0.556	5938	0.98	676	157	59.4 ± 4.2	2.23 ± 0.07	2.51 ± 0.07	0.89 ± 0.04	ND
18–19	–	–	–	–	–	–	1.91 ± 0.06	2.15 ± 0.06	0.89 ± 0.04	ND
24–25	–	–	–	–	–	–	1.95 ± 0.05	1.98 ± 0.05	0.99 ± 0.04	ND
Station: JL7; 24.4057°N, 118.1076°E; Depth = 12.0 m; $T = 28.4$ °C; $S = 27.8$; *TSM = 46 mg l^{-1}										
Bottom water	–	1984	8.8	6.6	18	0.47 ± 0.03	0.90 ± 0.04	1.79 ± 0.06	0.50 ± 0.03	–

0–0.5	0.662	2527	3.7	118	147	30.3 ± 4.0	1.69 ± 0.04	1.95 ± 0.04	0.87 ± 0.03	ND
0.5–1	0.686									ND
1–2	0.716	2857	1.0	134	152	30.3 ± 3.7	1.50 ± 0.04	1.45 ± 0.03	1.03 ± 0.04	ND
2–3	0.725	3168	1.1	189	160	42.7 ± 4.9	1.45 ± 0.04	1.36 ± 0.03	1.06 ± 0.04	ND
3–4	0.704	3523	1.1	152	179	70.5 ± 6.0	1.58 ± 0.04	1.69 ± 0.04	0.94 ± 0.03	ND
4–5	0.633	4150	1.3	160	178	70.6 ± 5.1	1.42 ± 0.03	1.59 ± 0.03	0.89 ± 0.02	ND
5–6	0.725	4831	0.77	194	151	64.3 ± 4.6	1.40 ± 0.04	1.54 ± 0.04	0.91 ± 0.03	ND
7–8	0.721	5903	0.55	288	227	65.7 ± 4.4	1.53 ± 0.05	1.54 ± 0.04	1.00 ± 0.04	ND
9–10	0.729	7077	0.94	379	188	36.2 ± 3.7	1.61 ± 0.05	1.51 ± 0.04	1.07 ± 0.04	ND
11–12	0.739	7872	0.51	465	236	17.6 ± 4.9	1.54 ± 0.04	1.49 ± 0.04	1.03 ± 0.04	ND
14–15	0.708	9145	0.53	636	345	77.8 ± 5.6	1.69 ± 0.05	1.66 ± 0.04	1.02 ± 0.04	ND
18–19	0.708	–	–	–	–	–	2.03 ± 0.04	1.90 ± 0.03	1.07 ± 0.03	ND

T and S represent temperature and salinity in the overlying water.

ND: Not measured or not detectable when the second measurement of sediment ^{234}Th is larger or indistinguishable from the first measurement.

* TSM denotes the average concentration of total suspended matter in the bottom water.

Appendix T2
^{224}Ra, DIC and nutrients in the water column of the Jiulong River estuary.

Station	Distance* (km)	Sampling time	Layer	Temperature (°C)	Salinity	TSM (mg l^{-1})	^{224}Ra dpm 100 l^{-1}	DIC (μmol l^{-1})	NO_3^- (μmol l^{-1})	NH_4^+ (μmol l^{-1})	H_4SiO_4 (μmol l^{-1})
Winter, 2014											
JL0	3.22	01/19/2014	Surface	15.1	0.2	–	117 ± 3.2	1299	162	205	288
JL1	10.99	01/18/2014	Surface	15.1	9.3	–	228 ± 6.5	1696	146	137	185
JL2	12.05	01/17/2014	Surface	14.3	6.7	–	206 ± 5.9	1635	156	185	224
JL3	16.41	01/15/2014	Surface	14.7	20.0	–	122 ± 3.3	1779	116	73	113
JL5	20.02	01/14/2014	Surface	14.9	23.9	–	81 ± 1.5	1900	85	29	71
JL6	24.10	01/13/2014	Surface	14.8	26.7	–	55 ± 1.6	1963	66	16	54
JL7	34.02	01/12/2014	Surface	15.0	24.9	–	64 ± 1.9	1959	67	16	54
Summer, 2014											
R	0.00	08/05/2014	Surface	30.4	0.0	16	25 ± 1.1	963	199	46	251
R	0.00	08/09/2014	Surface	31.8	0.0	17	20 ± 0.9	771	199	65	257
JL0	3.22	08/14/2014	Surface	30.1	0.0	74	53 ± 2.3	898	217	144	114
JL1	9.37	08/05/2014	Surface	31.4	0.0	31	23 ± 1.0	770	204	67	262
JL1	9.37	08/09/2014	Surface	31.7	0.0	46	20 ± 1.0	703	237	74	291
JL1	9.37	08/15/2014	Surface	29.6	0.0	48	67 ± 3.0	825	225	110	122
JL2	12.05	08/05/2014	Surface	31.5	1.3	54	49 ± 2.2	903	191	77	255
JL2	12.05	08/09/2014	Surface	31.8	1.0	55	45 ± 1.9	798	197	65	252
JL2	12.05	08/13/2014	Surface	30.6	0.1	246	71 ± 2.5	976	173	135	103
JL3	16.41	08/05/2014	Surface	32.5	5.6	26	76 ± 2.2	1054	172	49	220
JL3	16.41	08/08/2014	Surface	31.4	19.8	28	166 ± 4.8	1649	82	24	101
JL4	15.39	08/10/2014	Surface	31.5	14.3	21	156 ± 3.7	1465	108	31	141
JL5	18.62	08/05/2014	Surface	32.2	5.5	29	79 ± 2.3	1268	140	37	174
JL5	18.62	08/07/2014	Surface	30.7	20.3	31	171 ± 6.4	1569	87	29	113
JL5	18.62	08/09/2014	Surface	31.9	15.8	45	154 ± 4.0	1471	95	36	140
JL6	24.10	08/05/2014	Surface	31.3	16.3	25	91 ± 2.4	1481	103	25	128
JL6	24.10	08/06/2014	Surface	30.7	21.5	34	122 ± 3.5	1609	58	23	104
JL6	24.10	08/09/2014	Surface	31.7	24.9	28	105 ± 3.1	1789	46	15	63
JL7	34.02	08/05/2014	Surface	31.1	23.5	34	101 ± 2.9	1714	62	16	78
JL7	34.02	08/09/2014	Surface	31.4	28.6	40	73 ± 3.1	1940	16	6.9	27
O	37.77	08/05/2014	Surface	29.8	27.7	26	58 ± 1.7	1847	36	7.5	46
O	37.77	08/05/2014	Bottom	29.4	29.5	50	55 ± 2.5	1950	16	5.3	23
O	37.77	08/09/2014	Surface	29.1	31.1	27	41 ± 1.8	1936	5.8	3.6	16
O	37.77	08/09/2014	Bottom	30.7	30.2	51	37 ± 1.7	1986	2.1	1.5	8.6

R is the river end-member station.
* Distance from the river mouth at St. R.

Appendix T3
DIC and nutrient concentrations in the subterranean estuary and in the bottom water of the Jiulong River estuary.

		DIC (μmol l^{-1})	NO_3^- (μmol l^{-1})	NH_4^+ (μmol l^{-1})	H_4SiO_4 (μmol l^{-1})
STE[a]	($N = 4$)	5013 ± 2170	3.0 ± 2.6	331 ± 150	550 ± 151
Estuary[b]	Winter ($N = 7$)	1788 ± 209	107 ± 46	85 ± 77	131 ± 90
	Summer ($N = 15$)	1607 ± 405	79 ± 74	36 ± 44	77 ± 49

[a] Data adopted from Wang et al., (2015).
[b] Averages of the measurements in the bottom water of the estuary.

REFERENCES

Aller R. C. (1977) *Influence of Macrobenthos on Chemical Diagenesis of Marine Sediments* (Ph. D. thesis). Yale Univ.

Aller R. C. (1980) Quantifying solute distributions in the bioturbated zone of marine sediments by defining an average micro environment. *Geochim. Cosmochim. Acta* **44**, 1955–1965.

Aller R. C. (2014) Sedimentary diagenesis, depositional environments, and benthic fluxes. In *Treatise on Geochemistry* (eds. H. D. Holland and K. K. Turekian), second ed. Elsevier, Oxford, pp. 293–334.

Aller R. C. and Cochran J. K. (1976) $^{234}Th/^{238}U$ disequilibrium in near-shore sediment: Particle reworking and diagenetic time scales. *Earth Planet. Sci. Lett.* **29**, 37–50.

Beck A. J., Charette M. A., Cochran J. K., Gonneea M. E. and Peucker-Ehrenbrink B. (2013) Dissolved strontium in the subterranean estuary - Implications for the marine strontium isotope budget. *Geochim. Cosmochim. Acta* **117**, 33–52.

Beck A. J., Rapaglia J. P., Cochran J. K. and Bokuniewicz H. J. (2007) Radium mass-balance in Jamaica Bay, NY: Evidence for a substantial flux of submarine groundwater. *Mar. Chem.* **106**, 419–441.

Bernat M. and Goldberg E. D. (1968) Thorium isotopes in the marine environment. *Earth Planet. Sci. Lett.* **5**, 308–312.

Berner R. A. (1980) *Early Diagenesis: A Theoretical Approach*. Princeton Univ. Press, New Jersey.

Beusen A. H. W., Slomp C. P. and Bouwman A. F. (2013) Global land–ocean linkage: direct inputs of nitrogen to coastal waters via submarine groundwater discharge. *Environ. Res. Lett.* **8**, 034035.

Boudreau B. P. (1997) *Diagenetic Models and their Implementation: Modelling Transport and Reactions in Aquatic Sediments*. Springer-Verlag, Berlin, Heidelberg, New York.

Burnett W., Bokuniewicz H., Huettel M., Moore W. and Taniguchi M. (2003) Groundwater and pore water inputs to the coastal zone. *Biogeochemistry* **66**, 3–33.

Cai P., Shi X., Hong Q., Li Q., Liu L., Guo X. and Dai M. (2015) Using $^{224}Ra/^{228}Th$ disequilibrium to quantify benthic fluxes of dissolved inorganic carbon and nutrients into the Pearl River Estuary. *Geochim. Cosmochim. Acta* **170**, 188–203.

Cai P., Shi X., Moore W. S. and Dai M. (2012) Measurement of $^{224}Ra:^{228}Th$ disequilibrium in coastal sediments using a delayed coincidence counter. *Mar. Chem.* **138**, 1–6.

Cai P., Shi X., Moore W. S., Peng S., Wang G. and Dai M. (2014) $^{224}Ra:^{228}Th$ disequilibrium in coastal sediments: Implications for solute transfer across the sediment–water interface. *Geochim. Cosmochim. Acta* **125**, 68–84.

Cai W.-J., Dai M., Wang Y., Zhai W., Huang T., Chen S., Zhang F., Chen Z. and Wang Z. (2004) The biogeochemistry of inorganic carbon and nutrients in the Pearl River estuary and the adjacent Northern South China Sea. *Cont. Shelf Res.* **24**, 1301–1319.

Cai W.-J., Wang Y., Krest J. and Moore W. (2003) The geochemistry of dissolved inorganic carbon in a surficial groundwater aquifer in North Inlet, South Carolina, and the carbon fluxes to the coastal ocean. *Geochim. Cosmochim. Acta* **67**, 631–639.

Cao W., Hong H. and Yue S. (2005) Modelling agricultural nitrogen contributions to the Jiulong River estuary and coastal water. *Global Planet. Change* **47**, 111–121.

Charette M. A., Buesseler K. O. and Andrews J. E. (2001) Utility of radium isotopes for evaluating the input and transport of groundwater-derived nitrogen to a Cape Cod estuary. *Limnol. Oceanogr.* **46**, 465–470.

Dai M., Wang L., Guo X., Zhai W., Li Q., He B. and Kao S.-J. (2008) Nitrification and inorganic nitrogen distribution in a large perturbed river/estuarine system: the Pearl River Estuary, China. *Biogeosciences* **5**, 1545–1585.

Dulaiova H., Camilli R., Henderson P. B. and Charette M. A. (2010) Coupled radon, methane and nitrate sensors for large-scale assessment of groundwater discharge and non-point source pollution to coastal waters. *J. Environ. Radioact.* **101**, 553–563.

Froelich P. N., Klinkhammer G. P. and Bender M. L., et al. (1979) Early oxidation of organic-matter in pelagic sediments of the Eastern Equatorial Atlantic: suboxic diagenesis. *Geochim. Cosmochim. Acta* **43**, 1075–1090.

Garcia-Orellana J., Cochran J. K., Bokuniewicz H., Daniel J. W. R., Rodellas V. and Heilbrun C. (2014) Evaluation of ^{224}Ra as a tracer for submarine groundwater discharge in Long Island Sound (NY). *Geochim. Cosmochim. Acta* **141**, 314–330.

Garcia-Orellana J., Rodellas V., Casacuberta N., Lopez-Castillo E., Vilarrasa M., Moreno V., Garcia-Solsona E. and Masqué P. (2013) Submarine groundwater discharge: Natural radioactivity accumulation in a wetland ecosystem. *Mar. Chem.* **156**, 61–72.

He M., Cai E., Wu Q., Jiang J., Lin S., Xu H., Liu Q., Zheng F. and Li R. (1988) Studies on the ecology of benthos in the Jiulong Jiang estuary (In Chinese with English Abstract). *Acta Ecol. Sin.* **8**, 133–139.

Moore W. S. (1996) Large groundwater inputs to coastal waters revealed by ^{226}Ra enrichments. *Nature* **380**, 612–614.

Moore W. S. (2010) The effect of submarine groundwater discharge on the ocean. *Annu. Rev. Mar. Sci.* **2**, 59–88.

Moore W. S. and Arnold R. (1996) Measurement of ^{223}Ra and ^{224}Ra in coastal waters using a delayed coincidence counter. *J. Geophys. Res.* **101**, 1321–1329.

Moore W. S. and Shaw T. J. (1998) Chemical signals from submarine fluid advection onto the continental shelf. *J. Geophys. Res.* **103**, 21543–21552.

Moore W. S., Beck M., Riedel T., van der Loeff M. R., Dellwig O., Shaw T. J., Schnetger B. and Brumsack H. J. (2011) Radium-based pore water fluxes of silica, alkalinity, manganese, DOC, and uranium: A decade of studies in the German Wadden Sea. *Geochim. Cosmochim. Acta* **75**, 6535–6555.

Moore W. S., Sarmiento J. L. and Key R. M. (2008) Submarine groundwater discharge revealed by ^{228}Ra distribution in the upper Atlantic Ocean. *Nat. Geosci.* **1**, 309–311.

Pai S.-C., Tsau Y.-J. and Yang T.-I. (2001) PH and buffering capacity problems involved in the determination of ammonia in saline water using the indophenol blue spectrophotometric method. *Anal. Chim. Acta* **434**, 209–216.

Rama and Moore W. S. (1996) Using the radium quartet for evaluating groundwater input and water exchange in salt marshes. *Geochim. Cosmochim. Acta* **60**, 4645–4652.

Rodellas V., Garcia-Orellana J., Masqué P., Feldman M. and Weinstein Y. (2015a) Submarine groundwater discharge as a major source of nutrients to the Mediterranean Sea. *Proc. Natl. Acad. Sci. U.S.A.* **112**, 3926–3930.

Rodellas V., Garcia-Orellana J., Masqué P. and Font-Muñoz J. S. (2015b) The influence of sediment sources on radium-derived estimates of Submarine Groundwater Discharge. *Mar. Chem.* **171**, 107–117.

Santos I. R., Burnett W. C., Dittmar T., Suryaputra I. G. N. A. and Chanton J. (2009) Tidal pumping drives nutrient and dissolved organic matter dynamics in a Gulf of Mexico subterranean estuary. *Geochim. Cosmochim. Acta* **73**, 1325–1339.

Santos I. R., Eyre B. D. and Huettel M. (2012) The driving forces of porewater and groundwater flow in permeable coastal sediments: A review. *Estuarine Coastal Shelf Sci.* **98**, 1–15.

Schulz H. D. and Zabel M. (2006) *Marine Geochemistry*. Springer-Verlag, Berlin, Heidelberg, New York.

Seeberg-Elverfeldt J., Schlüter M., Feseker T. and Kölling M. (2005) Rhizon sampling of pore waters near the sediment/water interface of aquatic systems. *Limnol. Oceanogr. Methods* **3**, 361–371.

Shaw T. J., Moore W. S., Kloepfer J. and Sochaski M. A. (1998) The flux of barium to the coastal waters of the southeastern USA: the importance of submarine groundwater discharge. *Geochim. Cosmochim. Acta* **62**, 3047–3054.

Swarzenski P. W., Porcelli D., Andersson P. S. and Smoak J. M. (2003) The Behavior of U- and Th-series Nuclides in the Estuarine Environment. *Rev. Mineral. Geochem.* **52**, 577–606.

Wang G., Wang Z., Zhai W., Moore W. S., Li Q., Yan X., Qi D. and Jiang Y. (2015) Net subterranean estuarine export fluxes of dissolved inorganic C, N, P, Si, and total alkalinity into the Jiulong River estuary, China. *Geochim. Cosmochim. Acta* **149**, 103–114.

Wang M. (2008) *Characteristics of Sediment Granularity, Element Geochemistry and their Significance for Identifying Sedimentary Dynamic Environment in the Jiulongjiang Estuary (In Chinese with English Abstract)*. Xiamen Univ, Master.

Xu M. and Li C. (2003) Characteristics of heavy minerals composition and distribution in sediment from Jiulong River Estuary. *Mar. Sci. Bull.* **22**, 32–40.

Associate editor: Claudine Stirling